



## RESEARCH ARTICLE

10.1029/2023MS004054

## Key Points:

- An Energy Exascale Earth System Model (E3SM) configuration is developed to integrate variable-resolution meshes with component advancements
- The two-way river-ocean coupling scheme developed in E3SM significantly improves the representation of river-ocean interactions
- The new coupled E3SM configuration provides insights into the nonlinear interactions between storm surge and river discharge during compound flooding

## Supporting Information:

Supporting Information may be found in the online version of this article.

## Correspondence to:

D. Feng,  
dongyu.feng@pnnl.gov

## Citation:

Feng, D., Tan, Z., Engwirda, D., Wolfe, J. D., Xu, D., Liao, C., et al. (2024).

Simulation of compound flooding using river-ocean two-way coupled E3SM ensemble on variable-resolution meshes.

*Journal of Advances in Modeling Earth Systems*, 16, e2023MS004054. <https://doi.org/10.1029/2023MS004054>

Received 5 OCT 2023

Accepted 10 APR 2024

## Author Contributions:

**Conceptualization:** Dongyu Feng, Zeli Tan, Darren Engwirda, James J. Benedict

**Formal analysis:** Dongyu Feng

**Investigation:** Dongyu Feng

© 2024 Battelle Memorial Institute and The Author(s). *Journal of Advances in Modeling Earth Systems* published by Wiley Periodicals LLC on behalf of American Geophysical Union. This article has been contributed to by U.S. Government employees and their work is in the public domain in the USA. This is an open access article under the terms of the Creative Commons Attribution-NonCommercial-NoDerivs License, which permits use and distribution in any medium, provided the original work is properly cited, the use is non-commercial and no modifications or adaptations are made.

## Simulation of Compound Flooding Using River-Ocean Two-Way Coupled E3SM Ensemble on Variable-Resolution Meshes

Dongyu Feng<sup>1</sup> , Zeli Tan<sup>1</sup> , Darren Engwirda<sup>2</sup> , Jonathan D. Wolfe<sup>2</sup> , Donghui Xu<sup>1</sup> , Chang Liao<sup>1</sup> , Gautam Bisht<sup>1</sup> , James J. Benedict<sup>2</sup>, Tian Zhou<sup>1</sup> , Hong-Yi Li<sup>3</sup> , and L. Ruby Leung<sup>1</sup> 

<sup>1</sup>Atmospheric, Climate, & Earth Sciences Division, Pacific Northwest National Laboratory, Richland, WA, USA, <sup>2</sup>Los Alamos National Laboratory, T-3 Fluid Dynamics and Solid Mechanics Group, Los Alamos, NM, USA, <sup>3</sup>Department of Civil and Environmental Engineering, University of Houston, Houston, TX, USA

**Abstract** Coastal zone compound flooding (CF) can be caused by the interactive fluvial and oceanic processes, particularly when coastal backwater propagates upstream and interacts with high river discharge. The modeling of CF is limited in existing Earth System Models (ESMs) due to coarse mesh resolutions and one-way coupled river-ocean components. In this study, we present a novel multi-scale coupling framework within the Energy Exascale Earth System Model (E3SM), integrating global atmosphere and land with interactively coupled river and ocean models using different meshes with refined resolutions near the coastline. To evaluate this framework, we conducted ensemble simulations of a CF event (Hurricane Irene in 2011) in a Mid-Atlantic estuary. The results demonstrate that the novel E3SM configuration can reasonably reproduce river discharge and sea surface height variations. The two-way river-ocean coupling improves the representation of coastal backwater effects at the terrestrial-aquatic interface that are caused by the combined actions of tide and storm surge during the CF event, thus providing a valuable modeling tool for better understanding the river-estuary-ocean dynamics in extreme events under climate change. Notably, our results show that the most significant CF impacts occur when the highest storm surge generated by a tropical cyclone meets with a moderate river discharge. This study highlights the state-of-the-art advancements developed within E3SM for simulating multi-scale coastal processes.

**Plain Language Summary** Compound flooding (CF) happens when rivers and oceans interact in the coastal zone. There are limitations in current models to accurately simulate these processes because of the insufficient resolutions in the computational meshes and lack of details on how rivers and oceans are connected. This study creates a comprehensive framework for the Energy Exascale Earth System Model (E3SM) and demonstrates its ability to simulate a specific compound flooding event in a Mid-Atlantic estuary. Our framework combines models of the atmosphere, land, river, and ocean, each with its own level of detail near the coastline to account for their different physical processes. Our results show that the E3SM framework can reproduce the river discharge and sea level variations reasonably well. By simulating the interaction between river and ocean, we can better understand the effects of coastal water on river discharge forced by tides and storm surges during the CF event. Our simulation reveals that CF is most significant when a tropical cyclone produces the highest storm surge but moderate river discharge. This study demonstrates the capability of the E3SM model to accurately simulate the detailed coastal processes.

### 1. Introduction

Coastal zones are characterized by interactive land-river-ocean processes across a wide range of spatiotemporal scales, featuring intensive biological productivity and ecological diversity between aquatic and terrestrial environments (N. D. Ward et al., 2020). These dynamic processes impact the coastal resiliency of human and natural systems and create evolving risks in response to climate change and sea level rise (SLR) (Hermans et al., 2023; Strauss et al., 2021), such as saltwater intrusion (Chang et al., 2011), coastal sediment resuspension (Bianucci et al., 2018), and various types of flooding (Sheng et al., 2022). Among these risks, flood hazards emerge as critical threats to coastal communities and infrastructure, resulting in devastating socio-economic losses in recent decades (Desmet et al., 2018). With the projected growth in population and coastal development and accelerated SLR conditions, human exposure to such risks is anticipated to increase dramatically (Neumann et al., 2015;

**Methodology:** Dongyu Feng, Zeli Tan, Darren Engwirda, Jonathan D. Wolfe, Donghui Xu, Chang Liao, Gautam Bisht, James J. Benedict, Tian Zhou

**Project administration:** Zeli Tan, Darren Engwirda, Gautam Bisht, Tian Zhou, L. Ruby Leung

**Software:** Dongyu Feng, Jonathan D. Wolfe, Donghui Xu, Chang Liao, Gautam Bisht, James J. Benedict, Tian Zhou, Hong-Yi Li

**Supervision:** Zeli Tan, Darren Engwirda, Gautam Bisht, Tian Zhou, L. Ruby Leung

**Validation:** Dongyu Feng, Darren Engwirda, Donghui Xu

**Visualization:** Dongyu Feng

**Writing – original draft:** Dongyu Feng, Zeli Tan

**Writing – review & editing:**

Dongyu Feng, Zeli Tan, Darren Engwirda, Donghui Xu, Chang Liao, Gautam Bisht, James J. Benedict, Hong-Yi Li, L. Ruby Leung

Tellman et al., 2021). Coastal flooding is caused by a range of factors, including heavy rainfall, extreme river flow from upstream, strong tide and storm surge, and even from the simultaneous interaction of multiple flood drivers (P. J. Ward et al., 2018). For example, excessive precipitation commonly co-occurs with storm surges during a tropical cyclone (TC) event (Gori et al., 2022), and their interactions can result in catastrophic flooding. The coastal zone compound flooding (CF), which has drawn significant attention recently (Feng et al., 2023; Santiago-Collazo et al., 2019; K. Xu et al., 2023), is the flooding caused by multiple flood drivers occurring near simultaneously.

Earth system models (ESMs) are typically used to simulate the hydroclimate and biogeochemical processes and predict their changes under diverse global warming scenarios at large scales (O'Neill et al., 2016). Recently, there has been a notable surge in the applications of ESMs to simulate fine-scale processes such as the coastal dynamics (Bambach et al., 2022; Ikeuchi et al., 2017). Compared with regional models (Deb, Sun, et al., 2023), ESMs—which integrate atmosphere, land, land ice, river, and ocean components—may provide a robust predictive understanding of the complex multi-scale coastal processes that account for the human-ecosystem interactions and the corresponding impacts on Earth's climate at the coastal interface (N. D. Ward et al., 2020). In the context of flood modeling, fully coupled ESMs can provide comprehensive representations of all individual flood drivers and capture their interactions. Each component is designed to handle specific drivers, such as precipitation in the atmosphere model, runoff in the land model and storm surge in the ocean model, while effectively accounting for their interactions with other relevant processes involving heat, energy, or sediment transport (Li et al., 2015, 2022).

However, the current generation of ESMs has several limitations for accurately modeling CF. One critical limitation is their coarse mesh resolution. The compounding impacts of a TC event and the associated flood drivers are sensitive to the spatial patterns (Gori et al., 2020), requiring atmosphere, land, river, and ocean models to resolve TC characteristics, surface runoff, river discharge, and tide and storm surge dynamics respectively at appropriate scales. However, typical ESMs operate at mesh resolutions of tens to hundreds of kilometers. The insufficient resolution (a) can cause underestimated coastal backwater propagation (Feng et al., 2022), (b) leads to under-resolved hydrologic features such as river networks, watershed boundaries, and coastal bathymetry (Eilander et al., 2020), and (c) can produce large biases in the simulated water level (Ikeuchi et al., 2017). In particular, while most ocean models could reproduce the total water level well along the coast and in the open sea (Muis et al., 2020), there are limited applications in extending ocean models to estuaries, which is critical for providing reasonable downstream boundary information for the land and river components (Zhang et al., 2023). Resolving estuarine dynamics requires high horizontal resolution to accurately represent the bathymetric variations and barotropic tidal waves. The latter is seldom included in global ocean models.

Despite the importance of the coupling between river and ocean in simulating coastal flooding, such river-ocean interaction is usually oversimplified or ignored in existing ESMs (Chandanpurkar et al., 2022). Typically, the river inputs to the ocean are treated as “one-way” fluxes, and the upstream propagation of momentum from the ocean and the interaction with river discharge are ignored (N. D. Ward et al., 2020). In regional models, two-way coupling is not uncommon (Chen et al., 2013) even though it is arguably not necessary because the river-ocean interface of regional models can be defined at upstream locations (typically where in situ sampled salinity is 0) to eliminate any oceanic influence (Xiao et al., 2021; Zhang et al., 2020). However, in the global application of ESMs, the river-ocean interface usually has to be positioned at the coastline due to a lack of water quality data sampling. The lack of two-way processes severely limits the model's ability to represent the exchange of water and materials between the adjacent water bodies as well as compounding effects from SLR and storm surge (Ikeuchi et al., 2017). There are an increasing number of studies that couple the oceanic processes to the large-scale river models by prescribing the water level information at the river downstream boundary (Eilander et al., 2020; Ikeuchi et al., 2017; Luo et al., 2017; Nasr et al., 2021; Yamazaki et al., 2012). These studies achieve reasonable representations of the coastal backwater effects of ocean tides and surges on blocking the river discharge and causing high water levels near river mouths (Yamazaki et al., 2012). However, as the water level data is obtained either from observations, offline simulations, or reanalysis data sets, the offline-coupled configuration neglects the non-linear discharge-surge-tide interactions (Eilander et al., 2020). On the ocean side, because the model considers the river-ocean interface as an inflow boundary, the flow toward such boundary will be reflected directly. But in low-lying watersheds, coastal water, as driven by the ocean tide and surge, may propagate upstream into the river network and cause energy dissipation. This behavior is commonly observed in coastal wetlands (Morton & Barras, 2011). Moreover, during a CF event, the backwater propagation impedes

river discharge to the ocean, which alters the influence of discharge on the local sea level. It remains poorly understood how much this mutual interaction will affect the local flood modeling (Dykstra & Dzwonkowski, 2020), for which a two-way river-ocean coupling is needed (Santiago-Collazo et al., 2019). To the best of our knowledge, the two-way coupling has not yet been implemented between the river and ocean components in any ESM.

The aforementioned limitations may be alleviated with recent advances in ESMs, including variable-resolution computational meshes in atmosphere (Zarzycki et al., 2014), river (Feng et al., 2022), and ocean models (Logemann et al., 2021; Mathis et al., 2022) and the implementation of global tidal models (Barton et al., 2022; Pal et al., 2023). These enhancements, along with the two-way river-ocean coupling, should be integrated into a unified framework with model meshes refined at their respective spatiotemporal scales. This unified approach improves the holistic representation of the processes and systems in the coastal environment.

This work describes the new capabilities developed within the US Department of Energy's Energy Exascale Earth System Model (E3SM) (Golaz et al., 2019, 2022) as part of a larger ongoing effort to represent the fine-scale coastal processes. Our study contributes to the ongoing improvements of E3SM by introducing a multi-scale, tri-grid configuration and a novel coupling pathway between the river and ocean components. To resolve the various scales relevant to the extreme TC events and the inherent processes at the coastal zone, the E3SM tri-grid configuration couples the atmosphere, land and river, and ocean components employing three separate variable-resolution meshes designed for each component to enhance the ability to preserve their respective physics accurately. This flexible framework also aims to seamlessly represent interactions among atmosphere, land, river and ocean components and incorporate their recent developments. In particular, we introduce a two-way coupling between the river and ocean components to better capture the interactive processes occurring at the river-ocean interface. To assess the performance of the developed capabilities, we use a river basin and estuary within the Mid-Atlantic region of the United States (US) as a testbed. We evaluate the effectiveness of the new coupling scheme in representing CF resulting from the combined impacts of a tropical cyclone event. This manuscript is organized as follows. In Section 2, we introduce our study domain, the fully coupled E3SM framework with an overview of each model component, the two-way coupling scheme, variable-resolution meshes, and the designed numerical experiments. The evaluation of the model performance and coupling schemes is provided in Section 3. The findings and limitations are discussed in Section 4, where we also provide implications for compound flood modeling and future directions for ESMs. Lastly, Section 5 provides the conclusion.

## 2. Materials and Methodology

### 2.1. Study Domain

We used Delaware River Basin (DRB) and Delaware Bay Estuary (DBE) as the study domain (Figure 1a). DRB and DBE are located in the US Mid-Atlantic coast. The Delaware River is approximately 531 km in length, the longest undammed river in the eastern US coastal plain, with DRB covering an area of 36,570 km<sup>2</sup> and contributing 58% of freshwater inputs to DBE (Whitney & Garvine, 2006). DRB has over 30 million residents and provides drinking water to 6% of the US population. DBE is a funnel-shaped tidal river estuary, which covers 2,030 km<sup>2</sup> in surface area and is roughly 18 km wide near the bay mouth and 0.3 km wide near Philadelphia (NOAA gauge 8545240) (Sharp, 1984). It has an average depth of 7 m with a ~8–15 m deep shipping channel navigating into the Wilmington-Philadelphia port (DiLorenzo et al., 1993). DBE is dominated by semidiurnal harmonic tidal constituents (M2 and S2) (Aristizábal & Chant, 2013). The tidal range gradually increases from 1.5 m at the bay mouth to 2.8 m at the Delaware River outlet. In situ observations used for model evaluation in DRB and DBE are listed in Table 1 for locations shown in Figure 1a.

The US Mid-Atlantic coast was heavily impacted by a number of TC events over the past 30 years as the occurrence of severe storm surge and heavy rainfall (Sun et al., 2021) resulted in extensive damage to coastal infrastructure and properties (Rappaport, 2000). Notably, Hurricane Irene, a destructive TC, made landfall on the US east coast on 27 August 2011. This event caused excessive rainfall (up to ~250 mm) within DRB (Figure 1b) and significant flooding in communities along the Delaware River and its tributaries. Hurricane Irene also generated strong winds, reaching up to ~105 km hr<sup>-1</sup> in the U.S. Mid-Atlantic region, and caused a peak storm surge of 1.8 m in DBE (Avila & Cangialosi, 2011). Additionally, the low-lying area of DRB experienced severe CF due to the combined effects of storm surge and high river discharge. The adverse consequence of Hurricane

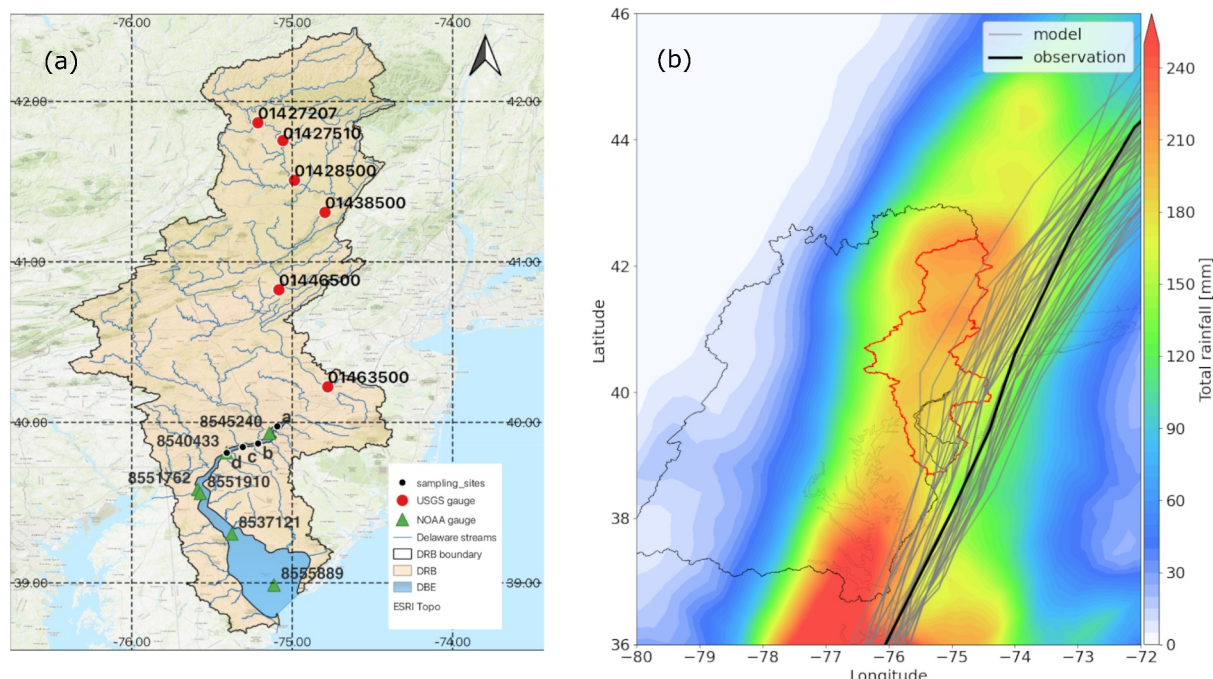


**Figure 1.** (a) An overview of Delaware River Basin (DRB), Delaware Bay Estuary (DBE) and gauge stations. (b) E3SM simulated Hurricane Irene tracks (gray lines), observed Irene track (black line), and ensemble mean storm total rainfall (color shading).

Irene thus highlights the vulnerability of the Mid-Atlantic region to TCs, particularly TC-induced CF (Kerns & Chen, 2023; Xiao et al., 2021; Ye et al., 2020).

## 2.2. E3SM Framework

We configured a multi-scale coupled framework based on E3SM version 2 (Golaz et al., 2022) that integrates the E3SM atmosphere model (EAM), E3SM land model (ELM), Model for Scale Adaptive River Transport (MOSART), and Model for Prediction Across Scales ocean model (MPAS-O) (Figure 2a). MOSART and MPAS-O are E3SM's river and ocean models, respectively. This configuration enables the full coupling of the atmosphere, land, river, and ocean components (Figure 2b). The fully coupled E3SM can simulate the key drivers for pluvial, fluvial, and coastal flooding, such as surface runoff, river discharge, and sea surface height (SSH). While

each individual component handles a specific type of flooding, the coupled framework enables the simulation of interactive CF processes. This advancement addresses the limitation of current CF simulations that rely on other models for boundary conditions and lack the ability to fully resolve the interactions between different flood drivers. It should be noted that this kind of CF simulation only becomes possible through collaborative efforts in mesh generation, input data preparation, climate data remapping, model development of two-way coupling, and new model configurations. The detailed information about each model component and the corresponding mesh is provided below.

### 2.2.1. Atmosphere Component

EAM is coupled in data mode, where atmospheric forcing is obtained from “pre-run” E3SM ensemble simulations of Hurricane Irene using E3SM version 2 (Figure 1b). E3SM supports a flexible data model as a dedicated data component that can efficiently read and handle large and complex data sets generated by E3SM simulations, enabling seamless data storage and retrieval of previous outputs. Although the atmospheric conditions generated

**Table 1**  
*Sources of Observation Data*

Station ID	Station name	Agency	Variable
01427207	Lordville	USGS	Discharge
01427510	Callicoon	USGS	Discharge
01428500	Lackawaxen	USGS	Discharge
01438500	Montague	USGS	Discharge
01446500	Belvidere	USGS	Discharge
01463500	Trenton	USGS	Discharge
8545240	Philadelphia	NOAA	Water level
8540433	Marcus Hook	NOAA	Water level
8551762	Delaware City	NOAA	Water level
8551910	Reedy Point	NOAA	Water level
8537121	Ship John Shoal	NOAA	Water level
8555889	Brandywine Shoal Light	NOAA	Water level

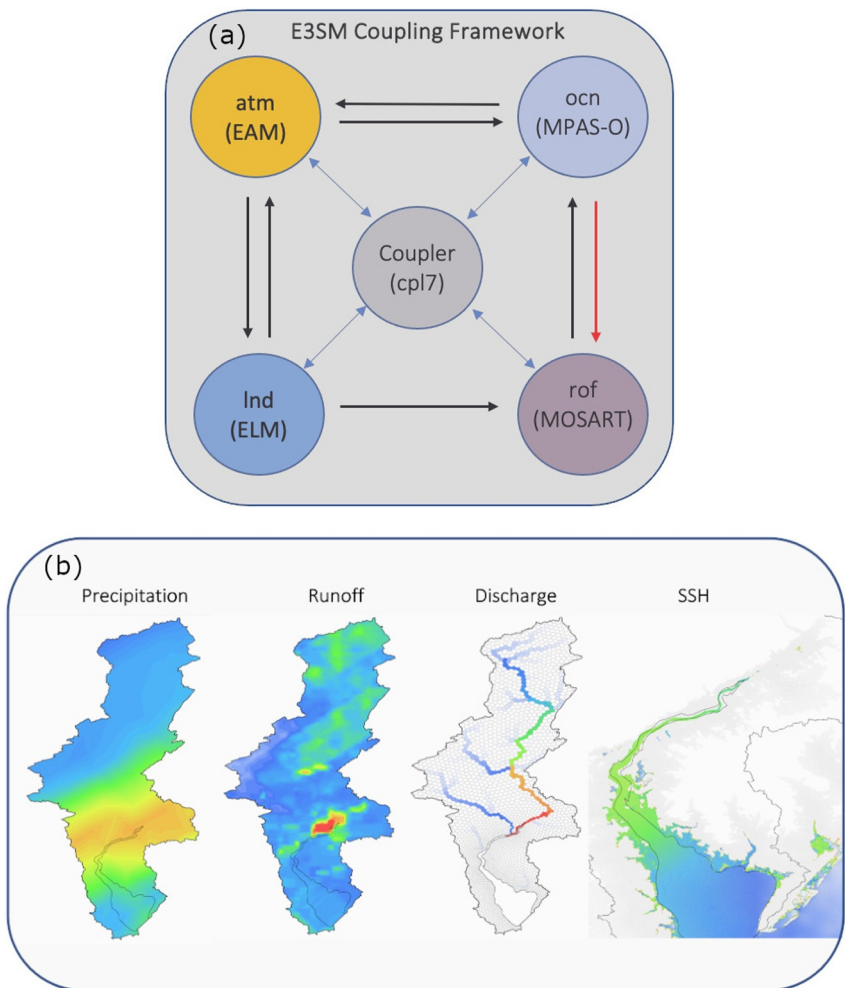


**Figure 2.** (a) The E3SM coupling framework. The red arrow represents the new linkage that enables the two-way river-ocean coupling. (b) An example of the flood drivers simulated by individual components of the E3SM framework.

by the “pre-run” E3SM simulations are used as forcing for subsequent runs that assess river runoff, such configuration is computationally efficient considering the higher computational expense in EAM simulations compared to the other components (Golaz et al., 2022). Moreover, this configuration allows us to select ensemble members based on prior analyses of the EAM output, ensuring a reasonable ensemble selection.

The pre-run E3SM ensemble simulations integrate prognostic atmosphere, land, and river model components with prescribed ocean sea surface temperature (SST) and sea ice cover (Huang et al., 2021). A detailed description of the ensemble configuration and validation is included in Appendix A of Deb, Benedict, et al. (2023), but summarized briefly here. While the river model is run on a global  $1/8^\circ$  mesh, the atmosphere, land, ocean, and ice components share a horizontal mesh regionally refined at  $\sim 25$  km over the North Atlantic Ocean and 100 km elsewhere (Figure 3, top left). Observed SSTs and sea ice concentrations interpolated to the model ocean grid are used to initialize the simulations and are held temporally constant, a simplification that is deemed adequate for analyses of sub-weekly hurricane analyses (Zarzycki & Jablonowski, 2015). EAM is initialized from ECMWF Reanalysis v5 (Hersbach et al., 2020), but no atmospheric nudging is applied. ELM and MOSART were spun up from a 1-year E3SM simulation forced by observed atmospheric conditions. Importantly, note that outputs from the river runoff and land models of these “pre-run” E3SM ensemble simulations are not analyzed in the present study. Only the first 10 days of the pre-run E3SM ensemble simulations are analyzed to assess the hurricane’s meteorological impacts. The hurricane ensembles were generated by perturbing physical parameters that TC simulations are most sensitive to He and Posselt (2015) and by varying the simulation initialization time. The parameters were perturbed by randomly selecting each value from a predefined range, resulting in a unique

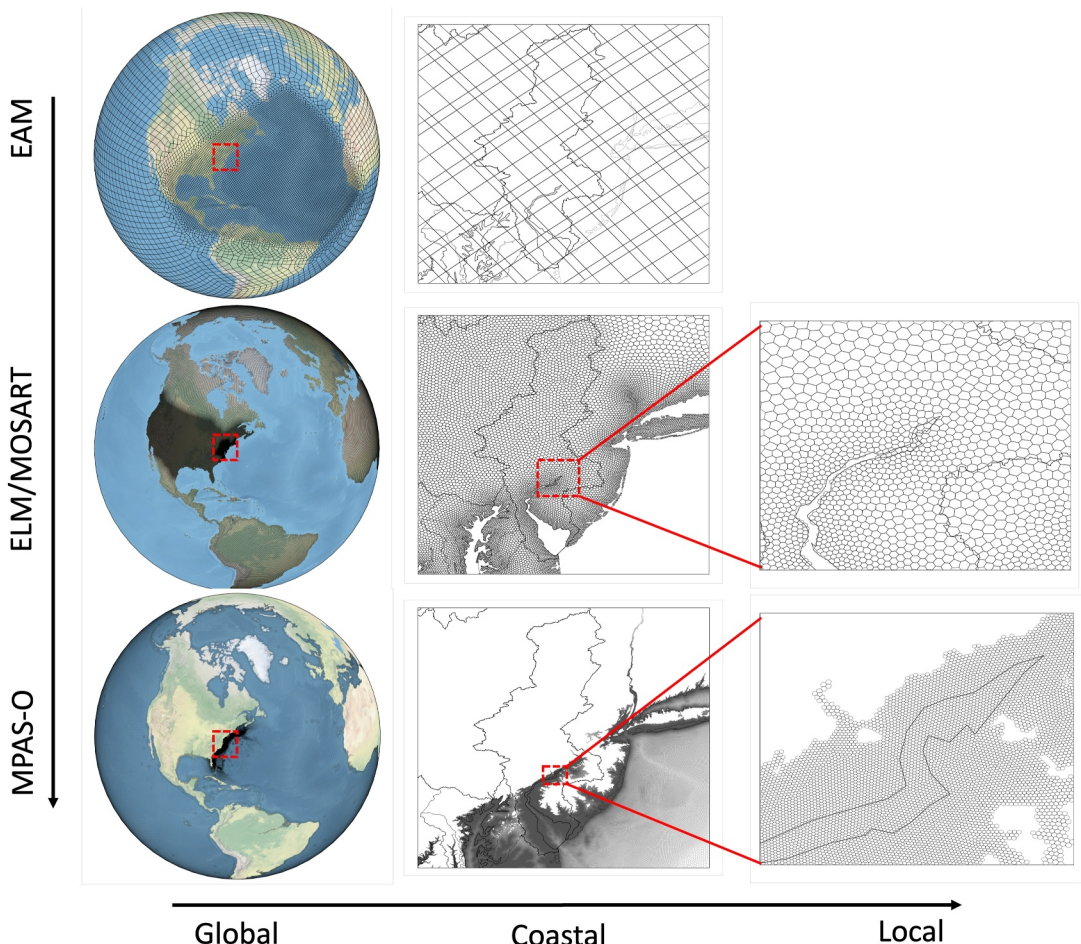


**Figure 3.** Global variable-resolution meshes for EAM, ELM, MOSART and MPAS-O with magnified views of the Mid-Atlantic coastal region and the Delaware River mouth. The boundaries of DRB and DBE are marked with black solid lines.

parameter set for each ensemble member. The initialization time was selected based on a sensitivity analysis of two initialization times separated by 12 hr, which indicated its effectiveness in capturing the precipitation and tracks of Hurricane Irene. Among all ensemble simulations, we adopted 25 ensemble members initialized at 00Z on 26 August 2011 (Figure 1b), which resulted in a reasonable distribution of hurricane characteristics. This ensemble approach accommodates our limited understanding of TC physics and effectively incorporates inherent uncertainties. Furthermore, each simulation produces a unique representation of the complex interactions between multiple flood drivers. These diverse scenarios offer valuable insights into the potential range of CF outcomes, enabling a more comprehensive assessment of the associated risks and impacts on coastal environments.

### 2.2.2. Land and River Component

In our configuration, ELM, MOSART, and MPAS-O are fully coupled, running on two different unstructured MPAS meshes (Figure 3). A critical advance of E3SM in resolving land, river and coastal processes is the use of separate variable-resolution meshes for land and ocean domains. We have successfully extended the unstructured Voronoi-type meshing workflow, widely employed in E3SM ocean and ice components, to provide an unstructured spatial discretization for land and river processes. The meshes are generated using the JIGSAW meshing library (Engwirda, 2017). Unlike the conventional strategies of using a hierarchy of nested submodels (Arellano & Rivas, 2019), our approach leverages the flexibility of the multi-scale E3SM to seamlessly embed high-resolution domains within a global configuration.

In our cases, the land mesh is refined to 3 km in the Mid-Atlantic watersheds but uses coarser resolutions of 30 km over the contiguous US domain and 60 km elsewhere. This mesh is also used by MOSART (i.e., river model) to

ensure one-to-one mapping of land runoff to river grid cells. Notably, this mesh is carefully aligned to match both the river topology and coastline. The complex river networks within the mesh are delineated by HexWatershed, a watershed boundary and flow direction delineation tool for large-scale river models (Liao, Zhou, Xu, Cooper, et al., 2023; Liao, Zhou, Xu, Tan, et al., 2023; Liao et al., 2022). We have configured MOSART with this mesh previously (Feng et al., 2022), which performed reasonably well in simulating the streamflow of the Delaware River. We spun up ELM and MOSART using a 10-year simulation forced by the Global Soil Wetness Projects version 3 (GSWPv3) climate forcing data set (Kim, 2017).

### 2.2.3. Ocean Component

The ocean component implements the recent developments in MPAS-O, including the single-layer barotropic version, the global tide model, a wetting-and-drying scheme, and a high-resolution (~250 m) mesh. The barotropic MPAS-O has been implemented in global tidal simulations (Barton et al., 2022; Pal et al., 2023) and a storm surge simulation along the Mid-Atlantic coast (Lilly et al., 2023). The tide model employed a full inline self-attraction and loading (SAL) calculation with a tuned wave drag and bottom drag coefficients and was evaluated globally against tidal prediction model TPXO8 (Egbert & Erofeeva, 2002) and gauged observations, and has shown comparable accuracy to the non-assimilative ocean models (Barton et al., 2022). The single-layer MPAS-O provides a reasonable approximation of the physics involved in tide and storm surge, as these processes are driven by tidal forcing, surface winds and air pressure rather than baroclinic motions (Mandli & Dawson, 2014). Compared with the default multi-layered MPAS-O, the barotropic configuration is computationally efficient and requires a much shorter spin-up time, thus allowing for higher resolutions in regions characterized by shallow depths and steep topographic gradients. We spun up MPAS-O with the tidal constituents applied for a month. Our ocean mesh has the finest resolution of 250 m along the US east coast and roughly 1 km outside this region (Figure 3). The mesh also covers partial land of the low-lying DRB, where the periodically flooded zone is handled using a wetting-and-drying scheme that accounts for subgrid-scale bathymetry/topography during coastal inundation.

### 2.2.4. E3SM Coupler

The communication between different model components is handled by the E3SM coupler (Craig et al., 2012). The coupler is the source code that drives the time step forward and connects model components. It controls the data flow and performs remapping, merging, diagnostics, and other calculations of states and fluxes. The coupler works in an online/offline fashion (Larson et al., 2005). In the offline phase, remapping files are generated for interpolating and intersecting variables between two model meshes. In the online phase, the E3SM coupler reads the weights in remapping files and data from the source model at runtime, performs rearrangement and interpolation, and sends remapped data to the destination model. These operations are performed every coupling period. In this study, we generated the remapping files for atmosphere/land, atmosphere/ocean, and river/ocean components using the remapping tools (Ullrich & Taylor, 2015; Ullrich et al., 2016; Zender, 2008). EAM (in data mode) is coupled with ELM and MPAS-O at a 15-min coupling interval, and MOSART is coupled with ELM and MPAS-O at a 1-hr interval, which is sufficient for the timescales of land runoff as well as ocean tide and surge and is consistent with the temporal frequency when sea level variation is imposed at the MOSART downstream boundary (Feng et al., 2022).

## 2.3. River-Ocean Two-Way Coupling

A downstream boundary was previously developed for MOSART (Feng et al., 2022), where in situ NOAA observations at the tidal gauge nearest to the river outlet were used as a surrogate of the ocean model and added as the Delaware River's downstream boundary conditions from an external boundary condition file. With the sea level variation enforced at the downstream boundary, the model performance is significantly improved for reproducing the water level at the backwater zone (Feng et al., 2022). However, as the backwater effects are solely constrained by the prescribed boundary condition, the effect of discharge on ocean dynamics is not represented. With the new developments in MPAS-O (Section 2.2), we are able to develop a two-way coupling between MOSART and MPAS-O to realistically represent the river-ocean interactions.

A new communication pathway is created in the E3SM coupler for MOSART and MPAS-O (Figure 2a). For a river outlet that has two-way coupling turned on, the water level from the nearest MPAS-O cell is used as the

	Experiment name	Atm forcing	Active component	River-ocean coupling
Model evaluation	<i>1way_baseline</i>	EAM	ELM → MOSART → MPAS-O	one-way
	<i>1way_datm</i>	GSPW JRA	ELM → MOSART	one-way
	<i>1way_r0125</i>	EAM	ELM (1/8°) → MOSART (1/8°)	one-way
Coupling evaluation	<i>2way</i>	EAM	ELM → MOSART → MPAS-O	two-way
	<i>1way_SSH</i>	EAM	ELM → MOSART ← SSH	one-way with CBC
	<i>1way_MSL</i>	EAM	ELM → MOSART ← MSL	one-way with CBC

**Figure 4.** Numerical experiments.

coastal boundary condition (CBC). Please refer to Appendix A and Feng et al. (2022) for more details. The rivers with two-way coupling turned off are one-way coupled to the ocean to eliminate the influence from other rivers. The two-way coupling enables MOSART to (a) receive water level information from MPAS-O at every coupling period to drive backwater propagation and characterize the hydrological response to tides and storm surges and (b) send the altered discharge back to MPAS-O (Chen et al., 2013). However, it should be noted that the two-way coupling is not appropriate for the river outlet if there are no adjacent ocean cells or the ocean model simulates the local water level poorly, in which case the two-way coupling may degrade the river model performance or lead to numerical instability. For example, a significant bias of simulated water level magnitude or phasing can result in incorrect river discharge.

#### 2.4. Numerical Experiments

A suite of numerical experiments (Figure 4) is performed to assess the model performance and different coupling schemes. While Experiment *1way\_datm* is forced by GSPW and JRA, the remaining configurations consist of 25 ensemble runs selected from the pre-run E3SM ensemble simulations of Hurricane Irene as noted earlier, resulting in a total of 127 simulations. The baseline configuration (*1way\_baseline*) is used to evaluate E3SM as introduced in Section 2.2 and includes all model components and the default one-way coupled MOSART and MPAS-O (Figure 4). The performance of MOSART and MPAS-O is assessed for streamflow at 6 USGS gauges along the mainstem of Delaware River and for water level at 6 NOAA tidal gauges across DBE (Figure 1), respectively, with evaluation metrics of coefficient of determination ( $r^2$ ), Kling–Gupta efficiency (KGE) (Gupta et al., 2009), and root mean squared error (RMSE).

The configurations of Experiments *1way\_datm* and *1way\_r0125* (Figure 4) are used to evaluate the impacts of hurricane-resolved ensemble atmospheric forcing and the regionally refined unstructured mesh on the MOSART performance. In both the configurations, MPAS-O is not activated. In Experiment *1way\_datm*, we used the regional-refined unstructured mesh for ELM and MOSART and two global reanalysis data sets, including GSPW (Kim, 2017) and Japan Meteorological Agency (JRA) (Kobayashi et al., 2015) with a 3-hr temporal resolution and a horizontal resolution of  $0.5^\circ$  and  $1.25^\circ$ , respectively. These atmospheric forcing data are commonly used for global land and ocean simulations over longer periods, but their applicability in simulating extreme events in regional studies is very uncertain. Thus, we use this experiment to demonstrate the importance of using hurricane-resolved ensemble atmospheric forcing in ESMs to capture extreme hydrological events during hurricanes. Experiment *1way\_r0125* implements the global  $1/8^\circ$  default mesh for ELM and MOSART. The mesh has a

**Table 2**  
*Mesh Statistics*

Model	Total horizontal cells	Resolution (km)
EAM	119,603	25–100
ELM/MOSART (unstructured)	166,355	3–60
ELM/MOSART (1/8°)	1,452,181	~12.5
MPAS-O	3,739,373	250–1

uniform resolution of ~12.5 km (Table 2) and was used in previous high-resolution E3SM simulations (Caldwell et al., 2019). This experiment tests the feasibility of running the land and river models on unstructured meshes at large spatial scales. We expect that the performance difference between Experiments *Iway\_baseline* and *Iway\_r0125* would be caused by not only the mesh resolution but also the improvements of river network representations with unstructured mesh.

The river-ocean coupling is assessed using the configurations of Experiments *2way*, *Iway\_SSH* and *Iway\_MSL* (Figure 4). We compare one-way coupling in the baseline case with two-way coupling and one-way coupling configurations but with a downstream CBC. The water level data prescribed at the MOSART CBC in Experiment *Iway\_SSH* is extracted from the MPAS-O simulated SSH in the baseline simulation. The impact of coupling schemes is estimated based on the difference in simulated river discharge ( $\Delta Q$ ) and SSH ( $\Delta \text{SSH}$ ):

$$\Delta Q = Q_c - Q_t, \quad (1)$$

$$\Delta \text{SSH} = \text{SSH}_c - \text{SSH}_t, \quad (2)$$

where  $Q$  and SSH are river discharge to the ocean and SSH simulated by MOSART and MPAS-O, respectively. The subscript  $c$  represents the baseline simulation and  $t$  is the test simulation. Experiment *Iway\_MSL*, in which the MOSART CBC is imposed with the mean sea level (MSL), is used as a reference for estimating the backwater effects (Feng et al., 2022), that is, the change in water depth ( $\Delta h$ ) and water volume ( $\Delta V$ ):

$$\Delta h(n,i) = h_{\text{exp}}(n,i) - h_{\text{MSL}}(n,i), \quad (3)$$

$$\Delta V(n,i) = \sum_i^N (h_{\text{exp}}(n,i) - h_{\text{MSL}}(n,i)) L(i) W(i), \quad (4)$$

where  $n$  is the model time step and  $i$  is the MOSART grid cell index,  $h$  is the water depth,  $V$  is the water volume in the river channel,  $L$  and  $W$  are the river channel length and width of the  $i$ th cell. The subscript  $\text{exp}$  represents the two-way coupled simulation and the one-way coupled simulation with the SSH CBC (i.e., *2way* and *Iway\_SSH*) and  $\text{MSL}$  represents Experiment *Iway\_MSL*. Finally, we use the backwater effects ( $\Delta V$ ) calculated from the two-way coupled simulation to quantify the impact of CF. This quantity measures the amount of backwater in the river channel driven by the river discharge, tide, storm surge and their interaction.

### 3. Results

Overall, the new E3SM configuration can simulate the river discharge and ocean SSH during Hurricane Irene reasonably well because the new variable-resolution meshing and the two-way coupling scheme provide a more reasonable representation of the river-ocean interactions.

#### 3.1. Model Evaluation

##### 3.1.1. MOSART

The MOSART simulated streamflow in the baseline simulation is validated against USGS observations at six Delaware River gauges during the 10-day Hurricane Irene period (Figure 5a). We calculated the ensemble mean streamflow and selected the “best” ensemble member that has the highest KGE averaged across all gauges. The measured streamflow generally falls within the ensemble spread. The spread in streamflow results from the variations in the hurricane track and rainfall distribution from the pre-run EAM ensemble simulations. The magnitude of peak flows is well captured by E3SM at the four downstream gauges (01428500 ~01463500) but is overestimated by 10%–20% at the two upstream gauges. The timing of the modeled peaks is slightly delayed relative to the observation, but the simulations align well with the observation for the streamflow recession. There are many factors that could contribute to the bias, including the uncertainty in the spatial distribution and timing of EAM-simulated precipitation, the ELM runoff generation, and the MOSART flow routing. Analyses presented in

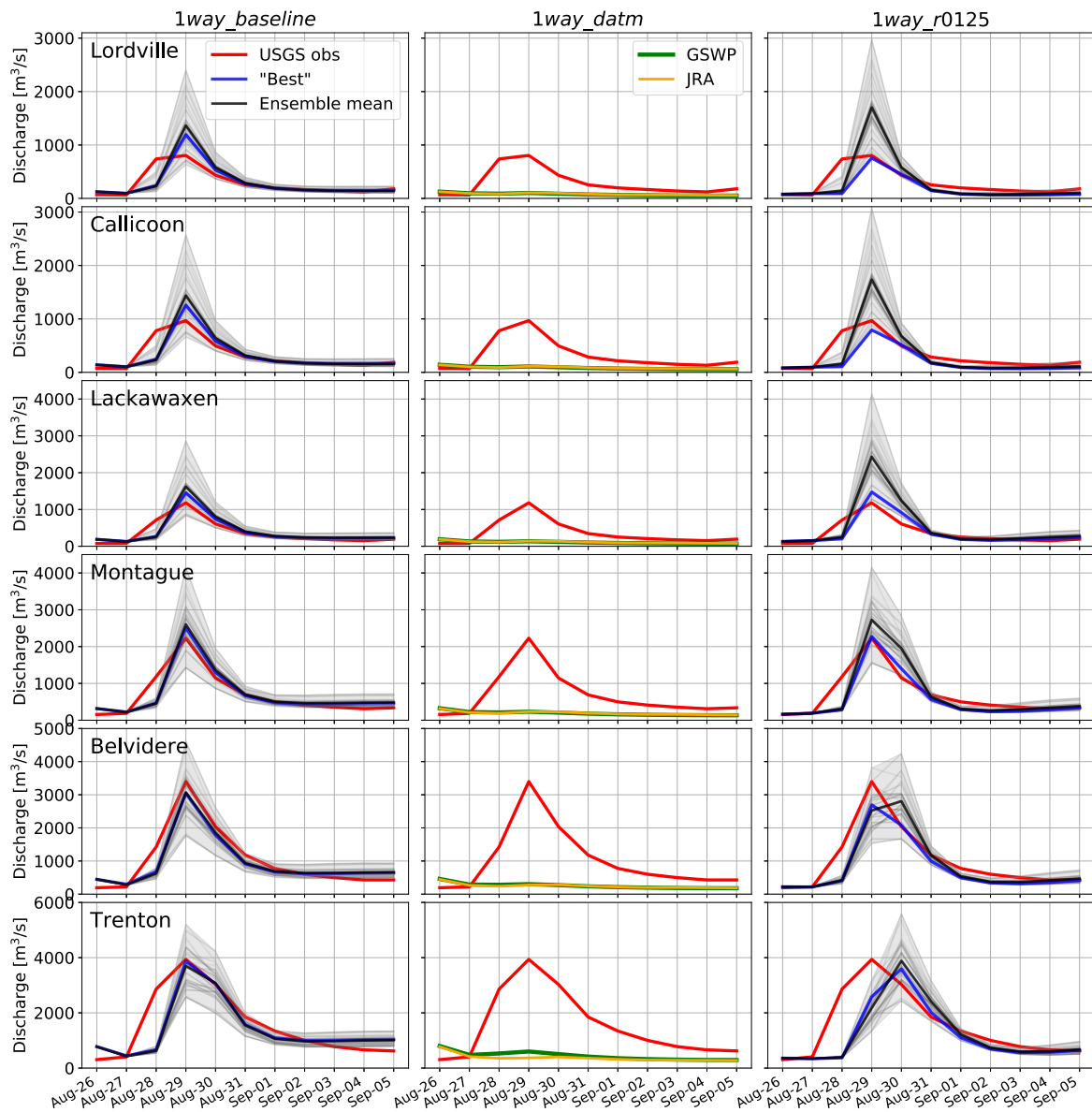


**Figure 5.** MOSART simulated streamflow at six USGS gauges in Delaware River during Hurricane Irene. The three columns represent the results from Experiments *1way\_baseline*, *1way\_datm* and *1way\_r0125*, respectively. “Best” refers to the ensemble member that has the highest skill scores of KGE averaged across all gauges.

(Deb, Benedict, et al., 2023) indicate that cumulative precipitation averaged across the larger HUC2 Mid-Atlantic watershed exhibits a delayed rainfall onset (underestimation by ~20% through 12Z on 28 August 2011) but an excessive storm-total rain amount (overestimation by ~33% through 12Z 29 August 2011). Our own analysis (not shown) also indicates that storm-total rainfall biases appear to be larger in the northern part of the DRB compared to the southern part. Together, these findings suggest that precipitation biases in the “pre-run” EAM ensemble contribute strongly to streamflow biases during Hurricane Irene. The amplified bias at the most downstream gauge (USGS 01463500) shows an aggregation of processes compared to other gauges. How the uncertainties propagate from the atmospheric forcing to the simulated streamflow needs further investigation in the future. Nevertheless, in the context of ESM, E3SM shows satisfactory performance in simulating an extreme event (Towner et al., 2019), with both  $r^2$  and KGE over 0.5 across all gauges (Figure 6).

More importantly, we use Experiment *1way\_datm* and *1way\_r0125* to demonstrate that the new configuration provides an improved performance of modeling extreme events compared to the default, original E3SM global

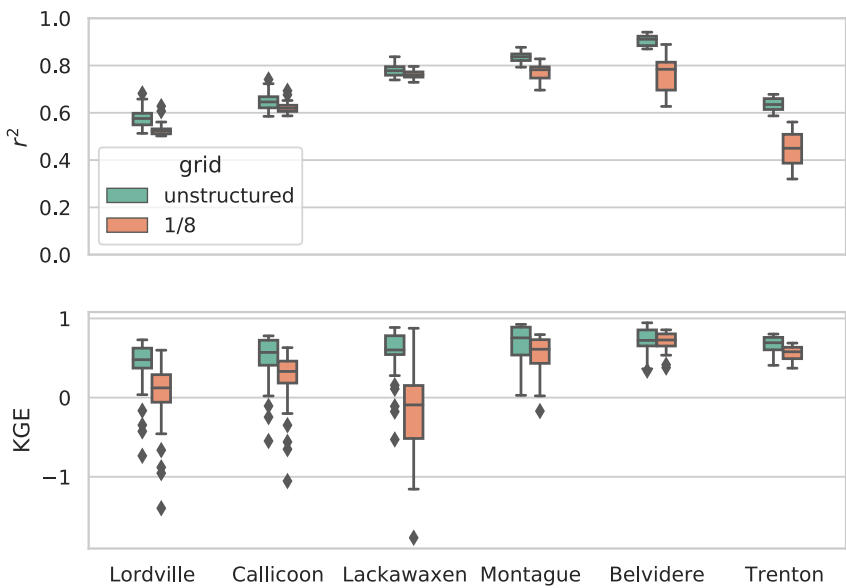


**Figure 6.** Whisker plot of the evaluation metrics of  $r^2$  and KGE for MOSART simulations using unstructured mesh and 1/8° uniform mesh at the six USGS gauges.

high-resolution configuration. Compared with the baseline experiment, the simulations in *Iway\_datm* fail to reproduce the streamflow peaks (green and yellow lines in Figure 5a), and the ensemble spread and the ensemble mean in *Iway\_r0125* overestimate the streamflow peaks across all gauges and predict more delayed peaks at two downstream gauges (Figure 5b). Because *Iway\_datm* is configured using the same unstructured mesh and initial condition as the baseline experiment but is forced by GSWP and JRA global atmospheric data, the poor model performance is caused by the use of the global atmospheric forcing. This is not unexpected because global reanalysis data sets are not calibrated for a single event. The total precipitation during Irene provided by GSWP and JRA both show intensive precipitation at downstream proportions of DRB (Figures S1 and S2 in Supporting Information S1), which explains the simulated flat hydrograph. Although this particular event should not be generalized or used to question the fidelity of such data sets, more attention should be paid when performing extreme event simulations using global climate data sets, especially in coastal watersheds. The simulations of *Iway\_r0125* also have reduced performance compared to the baseline (Figure 6). Specifically, the KGEs of *Iway\_r0125* are much lower than that of the baseline experiment at the three upstream gauges due to the poorly simulated peaks. As both *Iway\_r0125* and *Iway\_baseline* experiments are forced by the Irene ensemble, the simulation differences are caused by the coarser ELM/MOSART mesh. For example, the low-resolution mesh used in *Iway\_r0125* may not resolve the river network and topology sufficiently well. Besides the mesh, the larger bias may also stem from land surface data and river model parameters (D. Xu, Bisht, Sargsyan, et al., 2022). While identifying the uncertainty sources is not our focus, this study shows that the new E3SM configuration outperforms the traditional ones and highlights a new path to improve the simulation of extreme event in ESMs.

### 3.1.2. MPAS-O

The MPAS-O can reproduce the tidal variations based on evaluation of its simulated SSH against the measurements at six NOAA tidal gauges in DBE (Figure 7). The simulated SSH agrees reasonably well with the measured data, similar to another MPAS-O application study of Hurricane Sandy that implemented a higher resolution mesh and more sophisticated local time stepping (Lilly et al., 2023). The metrics of  $r^2$  and RMSE (Figure 8) suggest that MPAS-O has comparable skills to other baroclinic global ocean models in simulating local tide and storm surge (Zhang et al., 2023). But its performance is generally worse than regional estuary models that use observed sea level at the continental shelf as boundaries (Deb, Sun, et al., 2023; Xiao et al., 2021). The MPAS-O modeled tidal phase is slightly shifted by  $\sim 2$  hr. The amplitude in sea level variation is underestimated by the model for the gauges closer to the DBE mouth where SSH is dominated by tide. The modeled SSH is more reasonable at the two upstream gauges near the Delaware River mouth as the tidal range is amplified upstream by the channel constriction (Wong & Sommerfield, 2009). The ensemble variation is

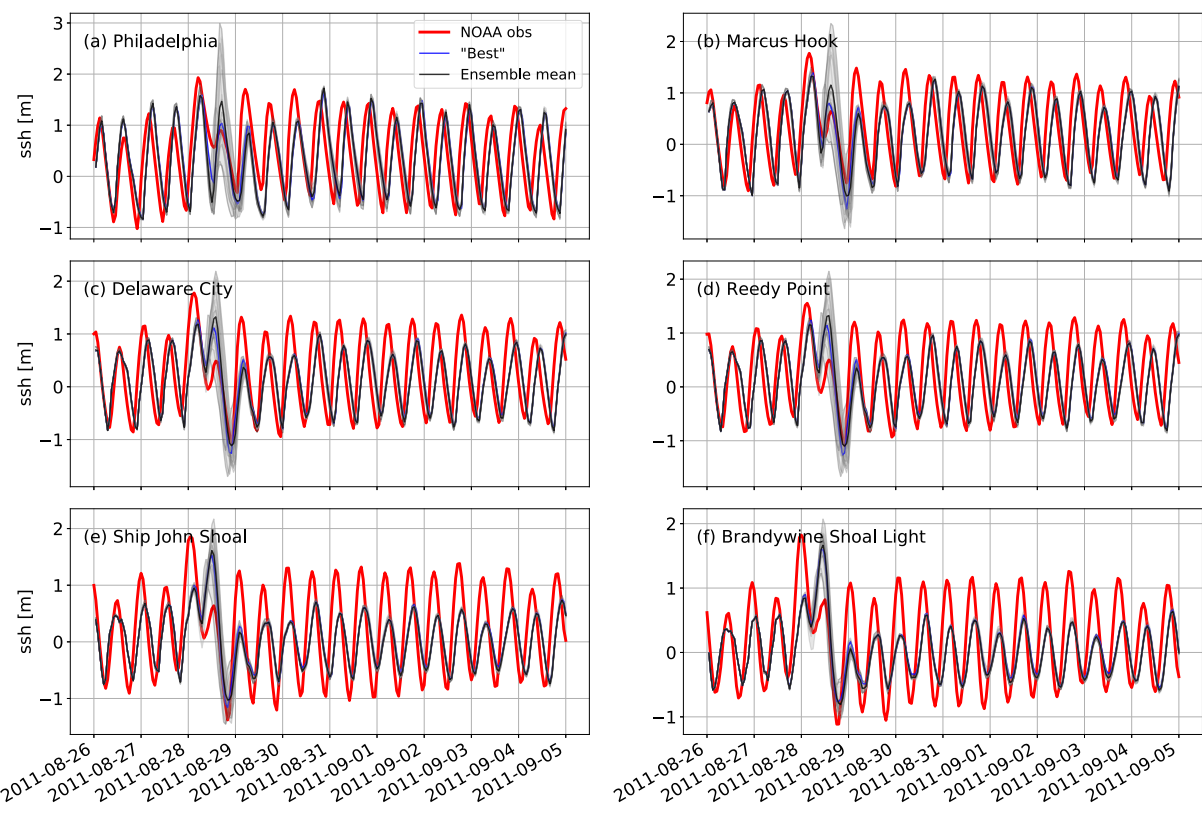


**Figure 7.** MPAS-O simulated SSH from Experiment *Iway\_baseline* at six NOAA tidal gauges in DBE during Hurricane Irene.

very small except during Hurricane Irene. Given that our EAM ensemble simulations involved parameter perturbations related to moist convection that ultimately altered the hurricane wind field, storm surge varies significantly from 1 m to a maximum of 3 m. The results show that the temporal variation of the simulated storm surge is generally consistent with the observation, especially for the ensemble mean (Figures 7a–7d), but

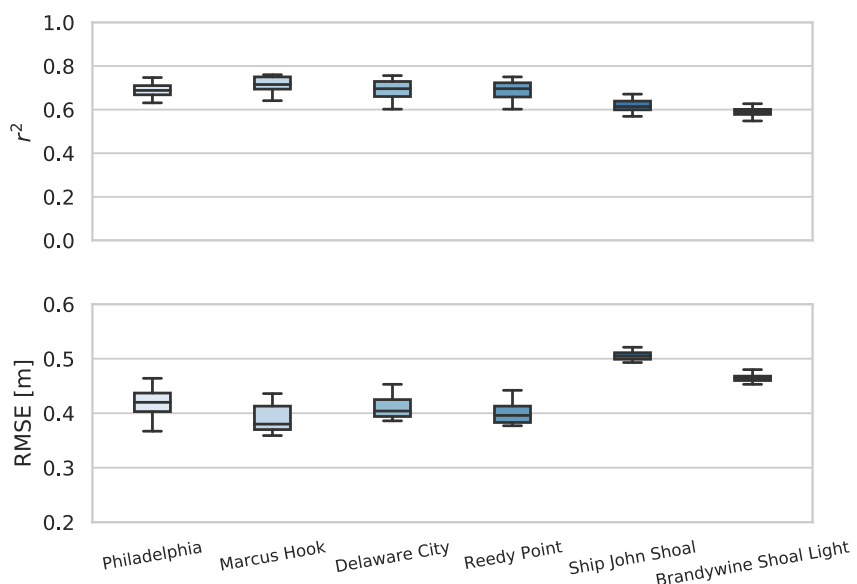


**Figure 8.** Whisker plot of the evaluation metrics of  $r^2$  and RMSE for MPAS-O simulations in Experiment *Iway\_baseline* at the six NOAA gauges.

the simulated largest ensemble spread is one day behind the storm surge peak. This delay is likely due to the underestimated forward speed of Hurricane Irene as simulated in the “pre-run” EAM ensemble. Although the predicted path of Hurricane Irene is reasonably accurate (cross-track errors, those perpendicular to the observed track, are  $\sim 20 - 40$  km), the EAM ensemble shows a larger along-track error—the component of error that is parallel to the observed hurricane track—of approximately  $-100$  to  $-150$  km indicating that the simulated storm is too slow. In the two gauges closer to the DBE mouth (Figures 7e and 7f), we simulated a greater “second” peak, which together with other SSH simulation biases, are likely due to the uncertainties in both EAM simulations and the configuration of MPAS-O.

There are still a few limitations in the current version of MPAS-O that impair the model prediction at the estuarine scale. A typical challenge for global ocean models is that the spatially varying bottom friction is usually not resolved in these models, and the bathymetry is usually sampled from less accurate global data sets, such as the General Bathymetric Chart of the Oceans (GEBCO), a global gridded bathymetric data set at roughly 450 m (Intergovernmental Oceanographic Commission (IOC) of UNESCO and International Hydrographic Organization (IHO), 2020). Thus, the MPAS-O performance may be further improved by merging higher-resolution coastal bathymetry for the DBE region. Nevertheless, overall the barotropic MPAS-O achieves a satisfactory performance at resolving estuarine dynamics and reproducing local tides and storm surges despite a medium added computational expense. The reasonable SSH predicted near the river mouth provides the basis for assessing the river-ocean coupling.

### 3.2. River-Ocean Coupling Evaluation

In this section, we evaluate different river-ocean coupling schemes by directly comparing one-way and two-way coupled simulations (e.g., *1way\_baseline* and *2way*), and the two-way coupled simulation and one-way coupled simulation but with a SSH CBC (e.g., *2way* and *1way\_SSH*).

#### 3.2.1. One-Way Coupling Versus Two-Way Coupling

The two-way coupled simulation shows the periodic variation in the hourly discharge  $Q_{\text{hourly}}$  at the river outlet (Figure 9a), ranging from  $-4,000$  to  $8,000 \text{ m}^3/\text{s}$ , which is caused by tide dynamics. For the river reach at the downstream Trenton (USGS 01463500), river flow is dominated by tides (Sharp, 1984), and the flow direction reverses with floods and ebb tides, as simulated by the two-way coupling, where the sign of  $Q$  changes at the tidal frequency. Negative  $Q$  implies an upstream propagating flow. In contrast, the streamflow variations of the one-way coupled simulation are purely driven by runoff and do not reflect the tidal effects. The tidally varied discharge implies that the two-way coupling scheme improves the representation of flow dynamics at the interface between a tidal river and ocean in E3SM, thus providing a more reasonable discharge for the ocean simulation.

The variation in  $\Delta Q$ , which reflects the direct impact of ocean on discharge, is consistent in correspondence to the SSH imposed at the MOSART CBC (Figure 9a). Generally,  $\Delta Q$  increases with SSH (Figure 9b), as a higher surge forces more backwater upstream that eventually contributes to river discharge during ebb tides, a mechanism leading to the greater oscillation of  $Q_{\text{hourly}}$ . The interaction between  $Q$ , tide, and storm surge is essentially a nonlinear process. However, the dynamics of  $\Delta Q$  are mainly governed by SSH at the river reaches close to the outlet, which explains the moderate linearity between  $\Delta Q$  and SSH.

The ocean-impacted  $Q$  extends to a significant range along the low-lying Delaware River, approximately 15–20 cells (or 40–70 km) upstream of the river mouth (Figure 9c). This extent is consistent with the range of river reaches where the backwater effects dominate (Feng et al., 2022) and is limited to the main channel where discharge is much larger. Although MOSART solves the simplified river dynamics and neglects the inertial acceleration, it can capture the backwater effects caused by tide and storm surge by prescribing the downstream coastal boundary.

Compared with  $Q_{\text{hourly}}$ , the daily discharge is usually more important for large-scale river modeling and the time scale of land and fluvial processes. Our comparison shows that the difference in  $Q_{\text{daily}}$  between the two simulations is much smaller than that of  $Q_{\text{hourly}}$  (cf. Figures 9a and 9b). But the difference ( $\Delta Q$ ) could still reach  $1,000 \text{ m}^3/\text{s}$  in a few ensemble members. Additionally, there is a forward shift of the hydrograph and an increase of the peaked  $Q_{\text{daily}}$  by up to  $1,000 \text{ m}^3/\text{s}$  by using the two-way coupling. These changes occur because storm surges

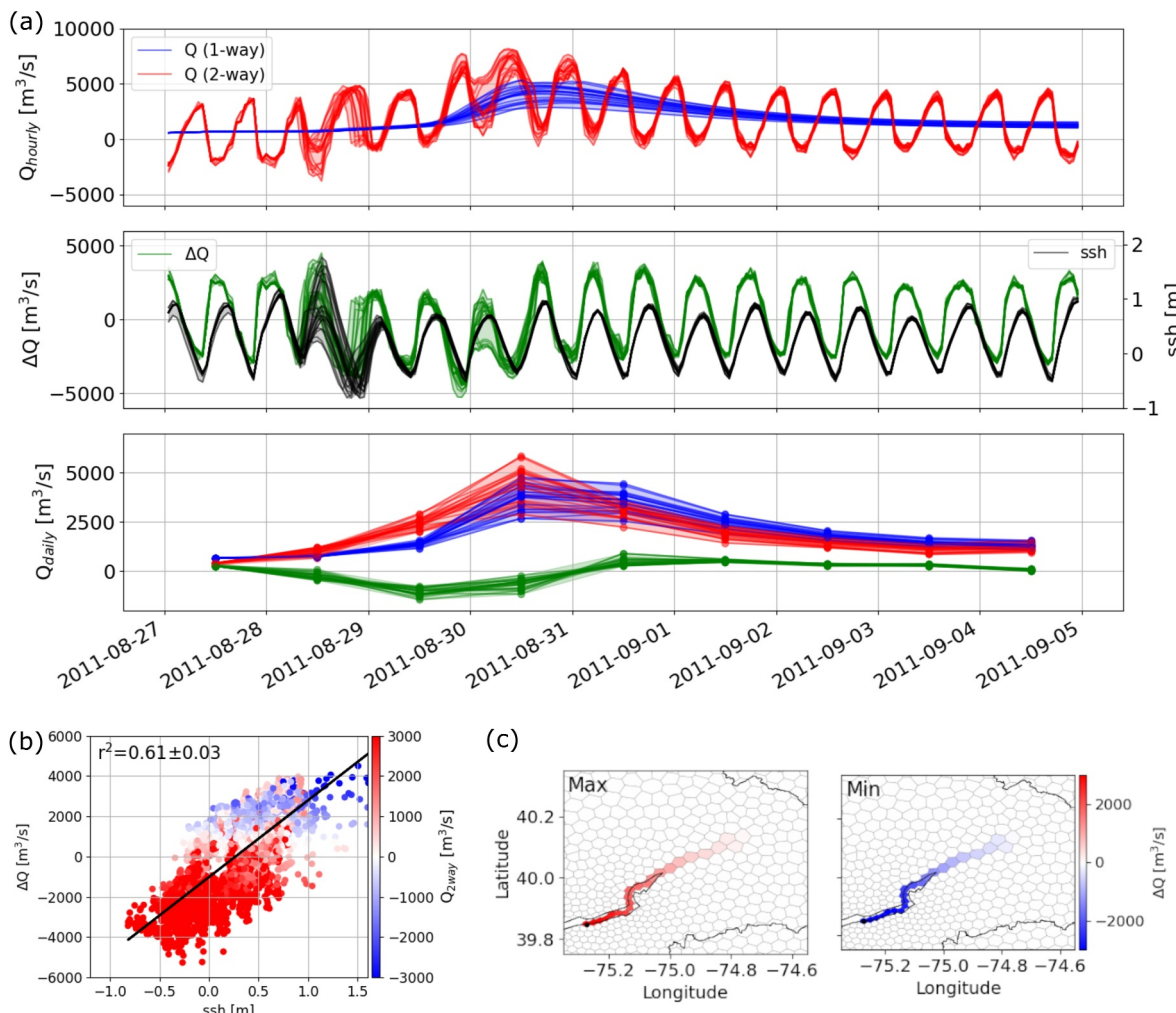


**Figure 9.** Comparison between one-way coupled and two-way coupled simulations (*Iway\_baseline* vs. *2way*). (a) Time series of MOSART simulated hourly discharge ( $Q_{\text{hourly}}$ ) and daily discharge ( $Q_{\text{daily}}$ ) at the river outlet, and their difference in  $Q$  ( $\Delta Q$ ) between the two experiments. The black line represents the SSH at the MOSART CBC from the two-way coupled simulation. (b) Scatter plot of  $\Delta Q$  against SSH. Colored circles represent the river discharge ( $Q$ ). SSH and  $Q$  are from Experiment *2way*. The black line is the fitted regression line to demonstrate the linearity. The mean value and the standard deviation of  $r^2$  are calculated for all ensemble members. (c) The maximum and minimum  $\Delta Q$  over the simulation period and across all ensemble members.

can force coastal backwater to the river channel, and correspondingly, the total amount of river discharge increases. Considering the magnitude and phasing of  $Q_{\text{hourly}}$ , the implementation of two-way coupling improves the representation of the modeled river discharge dynamics in the tidal river environment.

We further evaluated the influence of two-way coupling on the MPAS-O simulated SSH (e.g.,  $\Delta \text{SSH}$ ). The main finding is that the impact of two-way coupling on SSH is much smaller than that on discharge. Specifically, the two-way coupled simulation produces lower SSH than one-way coupled simulation during the storm surge event and all tidal cycles, which causes generally positive  $\Delta \text{SSH}$  (Figure 10). The reduced SSH results from the improved representation of the inflow boundary. During high storm surges and/or tides, the propagation of momentum from the ocean either impedes the river to flow downstream or even forces the river to flow upstream (Figure 9a). The reduced or negative discharge would lower the estuary water level. During ebb tides, the river flow is relatively enhanced due to both the tidal return flow and extreme runoff, which then contributes to the substantial increase in total discharge. This increased discharge generates extra inertial forcing that drives more water out of the bay and into the coastal ocean and correspondingly the local SSH near the river mouth is reduced. Such dynamics are only resolved in the two-way coupled simulation that enables a more realistic inflow boundary condition of tidal rivers in MPAS-O.

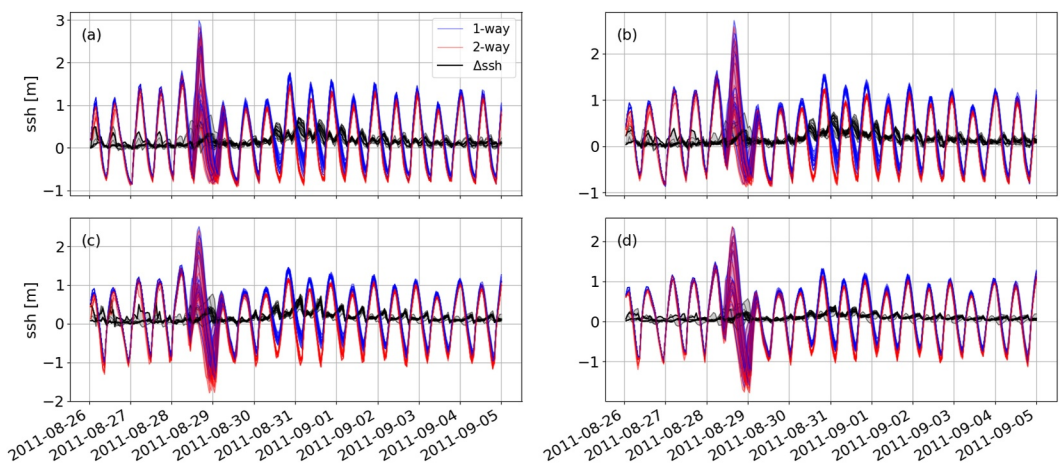


**Figure 10.** Time series of MPAS-O simulated SSH in one-way (*Iway\_baseline*; blue lines) and two-way (2way; red lines) coupled simulations as well as their difference ( $\Delta\text{SSH}$ ; black lines) at four sites located near the MOSART river outlet (Figure 1a).

Moreover,  $\Delta\text{SSH}$  responds to the increase of  $Q_{\text{Iway}}$ —the river discharge directly from the total runoff—roughly in a positive linear way (Figure 11). The consistent variation of  $\Delta\text{SSH}$  with  $Q_{\text{Iway}}$  is also shown in the time series comparison (Figure 10). The peaks in  $\Delta\text{SSH}$  coincide with the fluvial flooding period (August 30–August 31). Along with  $Q_{\text{Iway}}$ , storm surge can also increase the magnitude of  $\Delta\text{SSH}$ , which is indicated by the rapid increase of  $\Delta\text{SSH}$  during the low flow period (August 28) in Figure 11. Thus, in extreme events, the implementation of two-way coupling becomes more important, particularly during intensified discharge or storm surge. Another interesting finding is that  $\Delta\text{SSH}$  at the more upstream sites (Figures 11a and 11b) is slightly different from that at the downstream sites (Figures 11c and 11d). The magnitude of  $\Delta\text{SSH}$  during ebb tides is generally higher at the two downstream sites, possibly because these sites are more strongly affected by both river runoff and tides. The

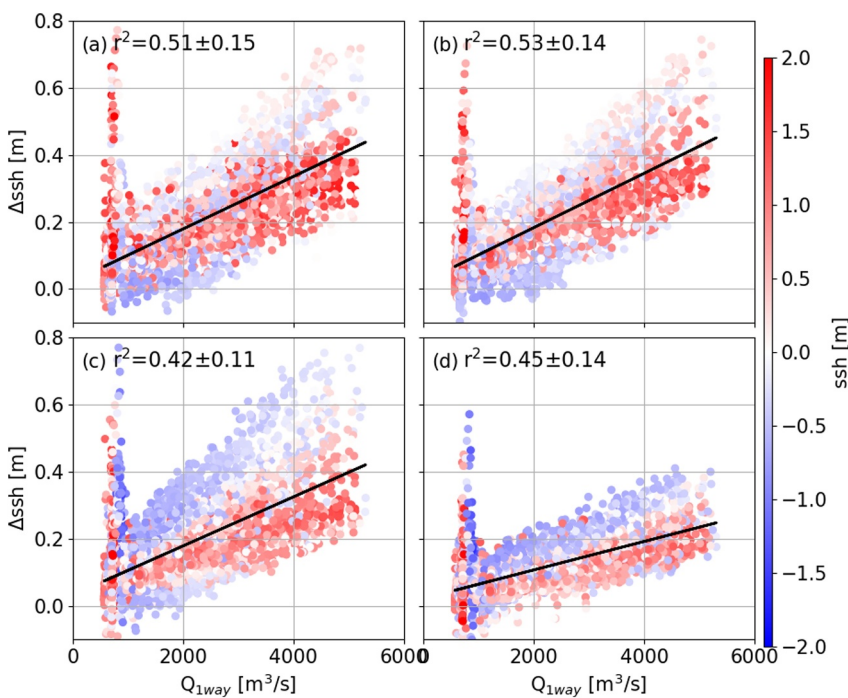


**Figure 11.** Scatter plot of  $\Delta\text{SSH}$  (computed from Experiments *Iway\_baseline* and 2way) against  $Q$  simulated in the one-way coupled simulation ( $Q_{\text{Iway}}$ ) at the four sampling sites. Colored circles represent SSH from Experiment 2way. The black lines are the fitted regression line. The mean value and the standard deviation of  $r^2$  are calculated for all ensemble members.

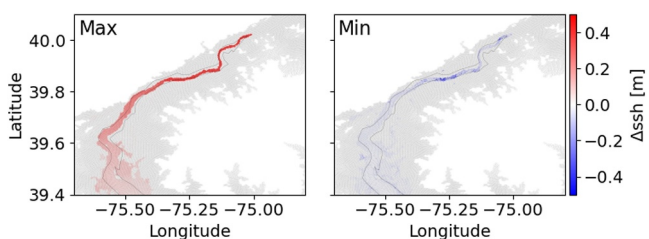


**Figure 12.** The maximum and minimum  $\Delta\text{SSH}$  (computed from Experiments *1way\_baseline* and *2way*) over the simulation period and across all ensemble members.

effective extent of the river-ocean coupling schemes in DBE can be recognized by the spatial variation of  $\Delta\text{SSH}$ , which gradually decreases from a maximum of  $\sim 0.5$  m near the river outlet and can extend into the upper and middle bay (Figure 12).

### 3.2.2. Two-Way Coupling Versus One-Way Coupling With CBC

In this section, we assess the merits of two-way coupling in comparison to the widely applied one-way coupling with CBC using Experiments *2way* and *1way\_SSH*. The two-way coupling scheme is evaluated in terms of backwater effects as quantified by  $\Delta h$  in Equation 3. Backwater effects are created by the elevated sea level, such as when the coastal water propagates upstream and

increases the water stage and fluvial flood risks in the coastal zone. We calculated the maximum increase in water level over the simulation period and among all ensemble members for both two-way coupled simulation ( $\Delta h_{2\text{way}}$ ) and one-way coupled simulation with SSH CBC ( $\Delta h_{1\text{waySSH}}$ ), as well as their difference. The spatial variation of  $\Delta h$  implies a clear difference in the magnitude, although the backwater extent is similar between the two schemes (Figure 13). The greater SSH in the one-way coupled simulation created a more intensive backwater propagation, with the water level greatly increased along the Delaware River by up to 0.4 m. This finding suggests a potential overestimation of compound effects in existing large-scale flood risk assessments, which relies on the one-way coupling method without accounting for the river-ocean mutual interactions.

The difference in the river discharge ( $\Delta Q$ ) is less significant than  $\Delta h$  between the two schemes. Both simulations are able to reproduce the tidal periodicity in  $Q_{\text{hourly}}$ , and the corresponding  $\Delta Q$  ranges from  $-2000$  to  $2000 \text{ m}^3/\text{s}$  (Figure 14a). Compared with the one-way coupled simulation, the two-way coupled simulation has slightly decreased flood and ebb peaks as well as shifted tidal phase. The simulated  $Q_{\text{daily}}$  is similar between the two simulations. Despite the different SSH imposed at the MOSART CBC, which is the main difference between the two simulations, there is not a notable correlation between  $\Delta\text{SSH}$  and  $\Delta Q$  (Figure 14b). This may be occurring because  $\Delta Q$  is influenced by additional factors, including the river discharge and its nonlinear interaction with SSH at the river-ocean interface. The spatial variation of  $\Delta Q$  is also not prominent (Figure 14c), but its upstream extent is similar to that in Figure 9c.

Overall, the implementation of two-way coupling demonstrates influential impacts on the modeling of both backwater effects and river discharge, particularly during extreme events. It should be noted that the biased discharge simulated in the one-way coupled scheme could increase the uncertainty of the downstream models that are sensitive to river inputs, such as biogeochemical and ecological models.

### 3.3. Compound Flood Modeling

The newly developed two-way coupled system in Experiment *2way* is applied to quantify the CF impact in terms of the daily change in water volume ( $\Delta V$ ) in the context of Hurricane Irene (Figure 15). We found that the CF impact is significant as  $\Delta V$  can reach up to 1/5 of the total discharge during the period (Figure 15). There are two peaks presented in  $\Delta V$  that are driven separately by storm surge and high discharge (Figure 15). With a medium discharge peak, higher levels of SSH correspond to greater  $\Delta V$ . In simulations with lower SSH but high and low discharge peaks, the variation of  $\Delta V$  is primarily affected by river discharge. Specifically, with a low discharge peak,  $\Delta V$  increases with the discharge. But with a high discharge peak,  $\Delta V$  shifts with the discharge. The latter

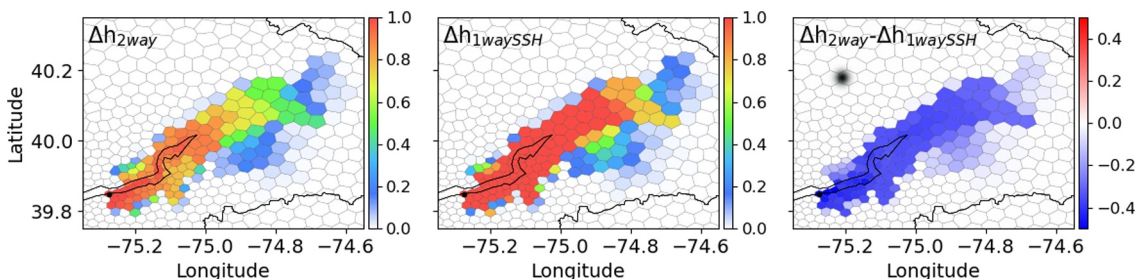


**Figure 13.** The maximum change in water depth of the two-way coupled simulation ( $\Delta h_{2\text{way}}$ ), one coupled simulation with SSH CBC ( $\Delta h_{1\text{waySSH}}$ ) and their difference.

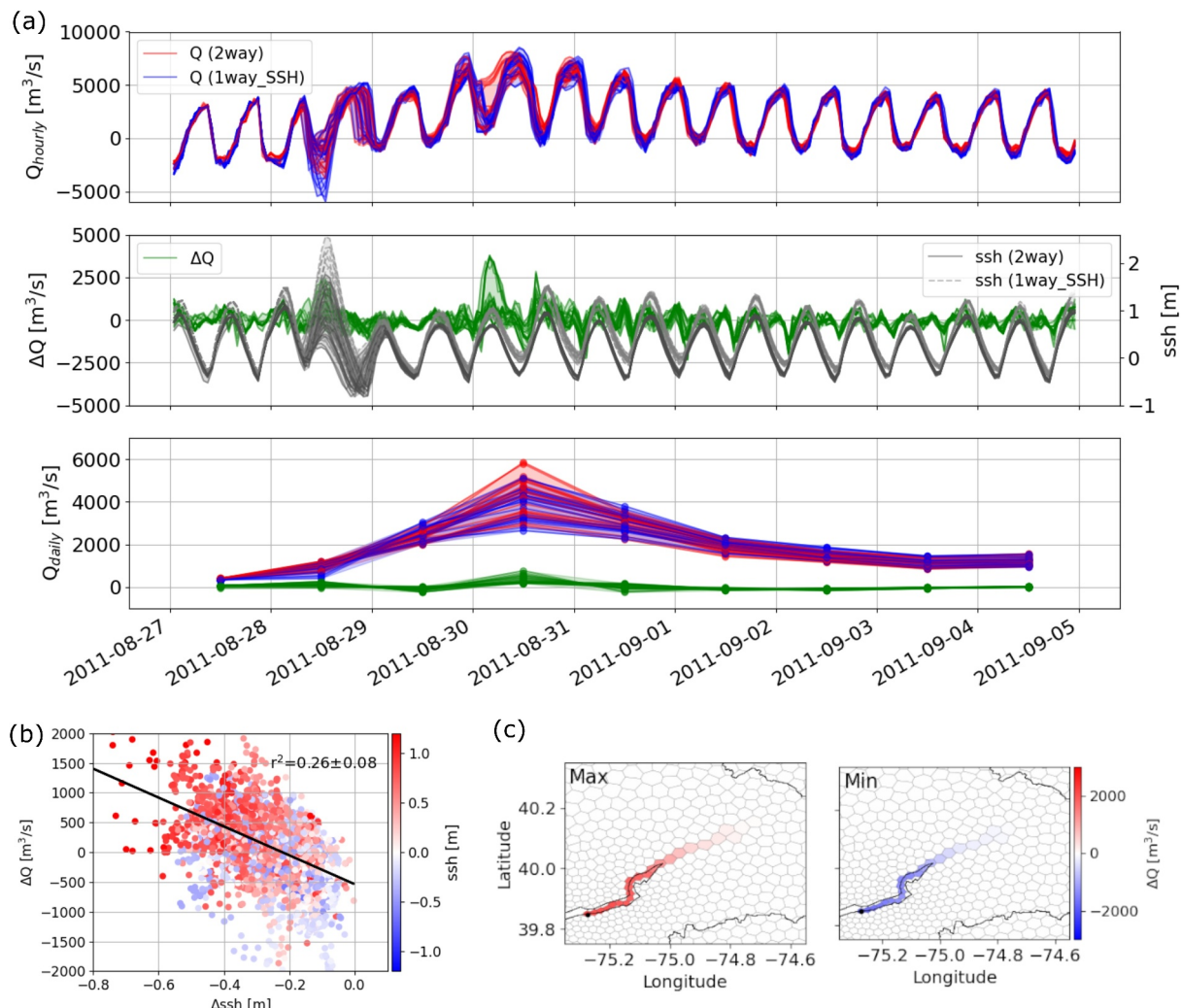


**Figure 14.** Comparison between the two-way coupled simulation and the one-way coupled simulation with SSH CBC (Experiment 2way vs. 1way\_SSH). (a) Time series of MOSART simulated hourly discharge ( $Q_{\text{hourly}}$ ), daily discharge ( $Q_{\text{daily}}$ ) and the difference in  $Q$  ( $\Delta Q$ ) between the two simulations. The black line and the gray line represent the SSH at the MOSART CBC from the two simulations. (b) Scatter plot of  $\Delta Q$  against  $\Delta \text{SSH}$ .  $\Delta \text{SSH}$  is the difference of SSH between the experiments. The colored circles represent SSH from Experiment 2way. The black lines are the fitted regression line to demonstrate the linearity. The mean value and the standard deviation of  $r^2$  are calculated for all ensemble members. (c) The maximum and minimum  $\Delta Q$  over the simulation period and across all ensemble members.

observation indicates that a substantial contribution of river discharge to the backwater volume can result in the attenuation of the backwater effect over an extended period. In general, the CF impact arises from the combined action of storm surge and high discharge, despite a limited overlap between the two drivers.

Subsequently, we computed the total  $\Delta V$ , total river discharge, and the maximum SSH during the simulation period for all 25 ensemble members (Figure 16). Each CF scenario is characterized by the corresponding total discharge and maximum SSH. The groups are organized as those in Figure 15. We found that the two flood drivers present a nonlinear impact on  $\Delta V$ . In the simulations with a low level of SSH (groups with high and low discharge peaks),  $\Delta V$  linearly increases with river discharge. However, under moderate discharge conditions (the group with medium discharge peak), SSH dominates and generates the most significant CF impacts, even in cases of low discharge. While our ensemble size is relatively small and does not include scenarios with simultaneous occurrence of a large storm surge and high discharge, our findings clearly show the nonlinear dynamics of CF caused by the interaction between fluvial and coastal flood drivers, as well as the dominating influence of storm surge in such events.

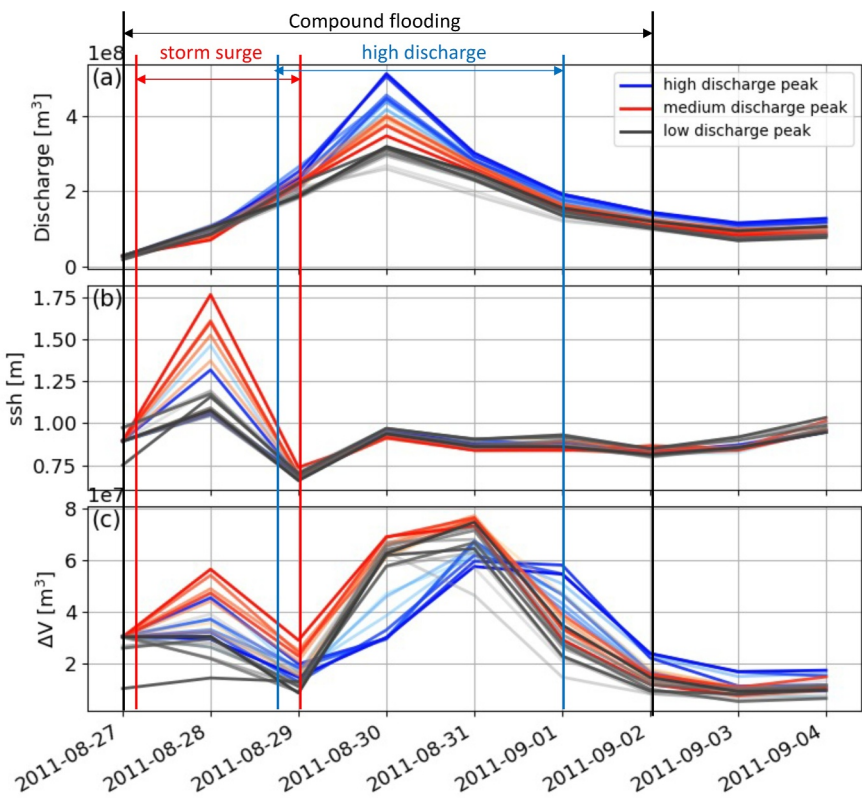


**Figure 15.** Time series of the accumulated amount of river discharge per day, daily maximum SSH and the daily change in water volume ( $\Delta V$ ). The ensemble members are categorized into three groups of high, medium and low discharge peaks. In the group with medium discharge peaks, darker colors refer to higher values of SSH, while in the other two groups, darker colors refer to higher discharge peaks.

#### 4. Discussion

Our numerical experiments summarize the enhanced capabilities of E3SM to reasonably capture the multi-scale physics within the coastal zone. In particular, the new E3SM coupled configuration shows improved performance over the current, widely used configurations in representing high river discharge during Hurricane Irene, which supports the use of ensemble atmospheric forcing, regionally refined unstructured meshes, and two-way river-ocean coupling in ESMs for coastal flooding studies. The barotropic MPAS-O is found to simulate reasonable water level fluctuations within the tidal river estuary in a computationally efficient way, which is important for resolving CF. The river-ocean two-way coupling improves the representation of interactive processes at the river-ocean interface.

##### 4.1. Importance of River-Ocean Coupling to Coastal Modeling

Our experiments demonstrate the substantial influence of the two-way river-ocean coupling on both river and ocean simulations. Through the coupling with coastal processes, the river model not only accounts for the backwater effects from tides and storm surges but also simulates more realistic discharge to the ocean, which in turn influences the ocean-simulated SSH within the estuary. In the two-way coupling, the change in SSH further affects the river simulation. This mutual interaction is neglected in the one-way coupling, which assumes the ocean modeled SSH is not affected by the change in river discharge. The backwater effects are constrained by the prescribed boundary

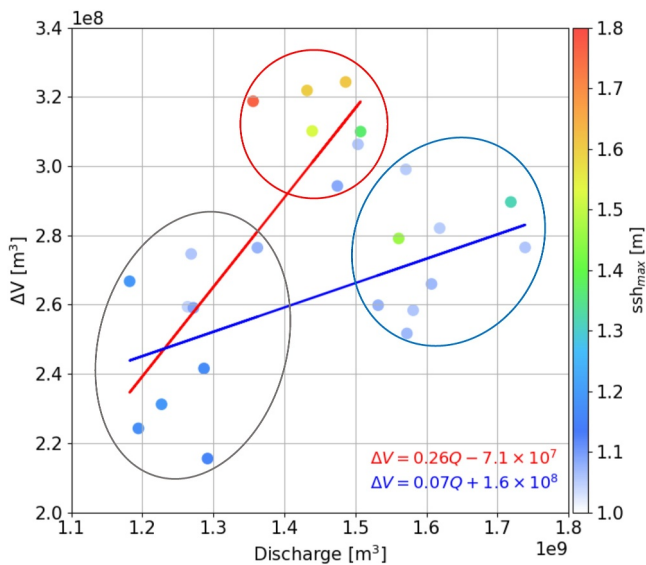


**Figure 16.** Scatter plot of total  $\Delta V$  against total discharge for 25 ensemble members. Both quantities are accumulated over the simulation period. Colored dots represent the corresponding maximum SSH. The three colored circles correspond to the groups in Figure 15. The two lines demonstrate the linear regression calculated from the combined groups.

condition. The two-way coupled simulation is inevitably more computationally expensive than the one-way coupling. In our configuration, while ELM and MOSART run efficiently and take only a few minutes to complete a 10-day simulation, MPAS-O is 20 times slower. The high computational cost of MPAS-O is caused by the high spatial resolution of model mesh (e.g., 250 m) and numerical schemes, which are necessary to capture the tidal dynamics. The computational cost is balanced by a significant expansion in capabilities, that is, the 2-way coupled variable-resolution tri-grid E3SM offers a pathway to modeling river-ocean dynamics globally and understanding sensitivities with respect to changing climate. The running cost of MPAS-O may be reduced with local time stepping method applied on variable-resolution meshes (Capodaglio & Petersen, 2022; Lilly et al., 2023).

Our comprehensive assessments of various river-ocean coupling schemes underscore the necessity of implementing two-way coupling to predict more realistic discharge of tidal rivers. The two-way coupling is of particular importance in capturing the hydrodynamic response of rivers to tides and storm surge. The two-way coupling is essential for reproducing the mutual impacts between river and ocean. It shows that ignoring these processes would lead to a biased assessment of compound flooding risks.

#### 4.2. Implications for Compound Flood Modeling

CF modeling in current large-scale river models typically uses a one-way coupled scheme (Eilander et al., 2020; Ikeuchi et al., 2017) to save computational cost from running the ocean model. These models can be applied at larger spatial domains in multiple flooding scenarios and produce accurate flooding maps (Karamouz et al., 2017). But such methods neglect the potential interactions between the flooding mechanisms in the flood transition zone (Bilskie & Hagen, 2018), such as precipitation-runoff, tide, and storm surge (Santiago-Collazo et al., 2019).

Our ensemble E3SM simulations provide valuable insights into CF, highlighting that CF is characterized by nonlinear interactions of different flood drivers rather than a mere superposition of fluvial and coastal flood drivers (Dykstra & Dzwonkowski, 2020). In our case, the most substantial CF effect occurred when the TC-generated highest storm surge coincided with a moderate discharge. However, it should be noted that such phenomenon may be unique to Hurricane Irene and the Delaware River because the occurrence and strength of each flood driver depend on hydrological conditions/regimes, geographical locations, and TC characteristics. For example, although discharge is primarily driven by precipitation, the magnitude of storm surge can be influenced by air pressure, wind speed and direction, and their interaction with local environments (Lin & Chavas, 2012). Importantly, the new capabilities in E3SM, including the variable resolution meshes and tri-grid configurations, enable the exploration of various types of flooding at a global scale within a unified system that seamlessly links the processes and interactions. As an efficient framework, the ensemble E3SM simulation of multiple TC scenarios would become achievable.

#### 4.3. Challenges and Future Work

With simple mesh refinement, E3SM can be used to simulate localized extreme events. However, the determination of river-ocean boundaries in various estuaries must be made locally. Considering the number of rivers globally and the change of geomorphological features over time, it is unrealistic to adjust the boundary for every river in ESMs, which requires the specification of different types of boundary conditions or coupling strategies (Chegini et al., 2022). This marks a crucial demand in our ongoing efforts to advance ESMs for better modeling of coastal processes. In this work, we have provided several alternatives for river-ocean coupling and are actively working toward expanding the range of available methods to accommodate a greater diversity of scenarios.

As the initial application of our E3SM development, there are certain limitations that we aim to address in future work. While MOSART and MPAS-O demonstrate reasonable performance, they exhibit slightly lower accuracy compared to regional models, so there is a need to further improve MOSART, MPAS-O, and their coupling. Uncertainty identification and quantification are needed regarding the model parameters and configurations, focusing on bathymetry data, tide model configuration, and bottom friction. In particular, the coarsely sampled global bathymetry have biases especially in shallower estuaries. While such data is commonly used in global ocean models, the simulation accuracy may be improved by using local bathymetry products at higher resolutions (Feng et al., 2019), such as 1-m USGS Coastal National Elevation Data (Danielson et al., 2018) or 1/9 arc-second Continuously Updated Digital Elevation Model (CUDEM) (Amante et al., 2023) in DBE, and 1/3 ~ 1 arc-sec data

from National Centers for Environmental Information (NCEI) along the Mid-Atlantic coast, and 3 arc-sec Coastal Relief Model in the deeper ocean (National Centers for Environmental Information, 2023). A possible uncertainty quantification approach is to conduct a model intercomparison study with higher-resolution regional coupled models. Additionally, the biases observed in the river and ocean simulations could be partly attributed to uncertainties in the atmosphere model. Although the EAM ensemble shows adequate performance in capturing Irene's track, it overestimates the hurricane's surface wind speeds and precipitation in the DRB region. The related uncertainties may have been propagated to the land, river, and ocean models, leading to the amplification of uncertainties. Such uncertainties may also be attenuated by other physical processes. Thus, in addition to an improvement of hurricane characteristics in the EAM ensembles, the uncertainty propagation through the multi-model framework warrants in-depth investigations.

Our proposed framework in this study would facilitate seamless integration of other new E3SM capabilities, including the lateral flow transport in the land subsurface (Qiu et al., 2023), land-river two-way coupling (D. Xu, Bisht, Zhou, et al., 2022), and land-ocean coupling, all of which will contribute to a fully coupled ESM with a more realistic representation of the land-river-ocean interaction. These processes vary across a range of spatio-temporal scales and are critical to global water and carbon cycling (Najjar et al., 2018; N. D. Ward et al., 2017), multi-variate flooding (Jongman et al., 2012), and land and marine transport of sediment and biogeochemical materials (Canuel & Hardison, 2016; Tan et al., 2021). Their global roles remain poorly quantified due to the limitations in the existing ESMs (N. D. Ward et al., 2020). This study provides the basis for an improved ESM framework to address these questions.

The refined E3SM could also be used to assess the impact of climate change on CF. A more general definition of CF is broadened to include the interaction of flood drivers and climate drivers (Zscheischler et al., 2020). The latter is related to decadal-scale climatic processes that may change the nature or distributions of flood drivers. For example, global warming contributes to enhanced tidal dynamics (Talke & Jay, 2020), the increase in storm intensity (Knutson et al., 2021), acceleration in SLR (Kulp & Strauss, 2019), and land use and land cover change (Deb, Sun, et al., 2023).

## 5. Conclusion

This study presents recent model developments incorporated into a unified framework to better represent multi-scale coastal processes in E3SM. The new capabilities include novel uses of variable resolution meshes, two-way coupled river-ocean components, and other enhancements in the E3SM ocean model. This framework is assessed using ensemble simulations of a tropical cyclone (TC) event with reasonable accuracy in the selected river and estuary domains. A two-way coupling between river and ocean components is developed within E3SM. This novel coupling methodology demonstrates its efficacy in capturing the interactive processes at the river-ocean interface. The two-way coupled ensemble simulations provide valuable insights into the CF modeling and reveal the nonlinear impacts of the river discharge and storm surge. The most significant CF impact is identified when the highest storm surge generated by a TC co-occurs with a moderate river discharge. This study demonstrates the state-of-the-art techniques in ESMs and emphasizes the overarching goal of resolving coastal dynamics within the E3SM framework. These advances in representing exchanges between the land, river, and ocean components of E3SM not only improve characterizations of hydrological response and the complex physical interactions across terrestrial-aquatic interfaces, but also provide a foundation for enabling interactive coupling of sediment and biogeochemical fluxes, interactions between water and biogeochemical cycles, and their response to human perturbations.

## Appendix A: River-Ocean Two-Way Coupling Scheme

This section provides details of the two-way coupling setup between MOSART and MPAS-O. In the conventional one-way coupling, the discharge flux of the one-dimensional (1-D) MOSART at each river outlet is provided to the nearest ocean cells of the two-dimensional (2-D) barotropic MPAS-O. In the same coupling period of the two-way coupled simulation, MPAS-O modeled SSH nearest to the river outlet will be imposed as MOSART's downstream coastal boundary condition (CBC) (Feng et al., 2022). In the two-way coupling configuration, MOSART applies diffusion wave equations for flow routing in the main channel. The momentum equation is expressed as

$$\frac{\partial h}{\partial x} - S_0 + S_f = 0,$$

where  $h$  is water depth,  $S_0$  is the river bottom slope and  $S_f$  is the friction slope. The Chezy-Manning equation is used to estimate the flow velocity ( $u$ ) in the open channel:

$$u = \frac{S_f}{|S_f|} \eta^{-1} R^{\frac{2}{3}} |S_f|^{\frac{1}{2}}, \quad (\text{A2})$$

where  $\eta$  is Manning's  $n$  coefficient,  $R$  is the hydraulic radius. At every grid cell,  $S_f$  is computed as

$$S_f(i) = \frac{h_{dstrm}(i) - h_c(i)}{\Delta x(i)}, \quad (\text{A3})$$

where  $h_c$  and  $h_{dstrm}$  represent the water depth of the current grid cell and the downstream cell, respectively, and  $\Delta x$  is the distance between the two cells and  $i$  is the cell index. At the outlet cell,  $h_{dstrm}$  is provided by MPAS-O during each coupling period.

## Data Availability Statement

The E3SM source code developed in this study is available at the Zenodo repository (Feng, 2024b). The water level data and streamflow data for model validations are publicly available via NOAA (<https://tidesandcurrents.noaa.gov/>) and USGS (<http://waterdata.usgs.gov/nwis/>) websites, respectively. The DRB subset of the E3SM ensemble simulation outputs with the variable fields used in the analysis is provided on Zenodo (Feng, 2024a).

## Acknowledgments

The work presented in this manuscript is supported by the Earth System Model Development program areas of the U.S. Department of Energy, Office of Science, Office of Biological and Environmental Research as part of the multi-program, collaborative Integrated Coastal Modeling (ICoM) project (Grant KP1703110/75415). All model simulations were performed using resources available through (a) Research Computing at Pacific Northwest National Laboratory (PNNL) and (b) the National Energy Research Scientific Computing Center (NERSC), a U.S. Department of Energy Office of Science User Facility located at Lawrence Berkeley National Laboratory, operated under Contract No. DE-AC02-05CH11231 using NERSC award BER-ERCAP m3780 for 2022. PNNL is operated for DOE by Battelle Memorial Institute, United States under contract DE-AC05-76RL01830. We appreciate the two anonymous reviewers for their critical assessment of our work.

## References

- Amante, C. J., Love, M., Carignan, K., Sutherland, M. G., MacFerrin, M., & Lim, E. (2023). Continuously updated digital elevation models (CUDEMs) to support coastal inundation modeling. *Remote Sensing*, 15(6), 1702. <https://doi.org/10.3390/rs15061702>
- Arellano, B., & Rivas, D. (2019). Coastal upwelling will intensify along the Baja California coast under climate change by mid-21st century: Insights from a GCM-nested physical-NPZD coupled numerical ocean model. *Journal of Marine Systems*, 199, 103207. <https://doi.org/10.1016/j.jmarsys.2019.103207>
- Aristizábal, M., & Chant, R. (2013). A numerical study of salt fluxes in Delaware Bay estuary. *Journal of Physical Oceanography*, 43(8), 1572–1588. <https://doi.org/10.1175/jpo-d-12-0124.1>
- Avila, L. A., & Cangialosi, J. (2011). *Tropical cyclone report, hurricane Irene, 21–28 August 2011*. U.S. National Hurricane Center. Retrieved from [http://www.nhc.noaa.gov/data/tcr/AL092011\\_Irene.pdf](http://www.nhc.noaa.gov/data/tcr/AL092011_Irene.pdf)
- Bambach, N. E., Rhoades, A. M., Hatchett, B. J., Jones, A. D., Ullrich, P. A., & Zarzycki, C. M. (2022). Projecting climate change in South America using variable-resolution community Earth system model: An application to Chile. *International Journal of Climatology*, 42(4), 2514–2542. <https://doi.org/10.1002/joc.7379>
- Barton, K. N., Pal, N., Brus, S. R., Petersen, M. R., Arbic, B. K., Engwirda, D., et al. (2022). Global barotropic tide modeling using inline self-atraction and loading in MPAS-ocean. *Journal of Advances in Modeling Earth Systems*, 14(11), e2022MS003207. <https://doi.org/10.1029/2022ms003207>
- Bianucci, L., Balaguru, K., Smith, R. W., Leung, L. R., & Moriarty, J. M. (2018). Contribution of hurricane-induced sediment resuspension to coastal oxygen dynamics. *Scientific Reports*, 8(1), 1–10. <https://doi.org/10.1038/s41598-018-33640-3>
- Bilskie, M., & Hagen, S. (2018). Defining flood zone transitions in low-gradient coastal regions. *Geophysical Research Letters*, 45(6), 2761–2770. <https://doi.org/10.1002/2018gl077524>
- Caldwell, P. M., Mametjanov, A., Tang, Q., Van Roekel, L. P., Golaz, J.-C., Lin, W., et al. (2019). The DOE E3SM coupled model version 1: Description and results at high resolution. *Journal of Advances in Modeling Earth Systems*, 11(12), 4095–4146. <https://doi.org/10.1029/2019ms001870>
- Canuel, E. A., & Hardison, A. K. (2016). Sources, ages, and alteration of organic matter in estuaries. *Annual Review of Marine Science*, 8(1), 409–434. <https://doi.org/10.1146/annurev-marine-122414-034058>
- Capodaglio, G., & Petersen, M. (2022). Local time stepping for the shallow water equations in MPAS. *Journal of Computational Physics*, 449, 110818. <https://doi.org/10.1016/j.jcp.2021.110818>
- Chandanpurkar, H. A., Lee, T., Wang, X., Zhang, H., Fournier, S., Fenty, I., et al. (2022). Influence of nonseasonal river discharge on sea surface salinity and height. *Journal of Advances in Modeling Earth Systems*, 14(2), e2021MS002715. <https://doi.org/10.1029/2021ms002715>
- Chang, S. W., Clement, T. P., Simpson, M. J., & Lee, K.-K. (2011). Does sea-level rise have an impact on saltwater intrusion? *Advances in Water Resources*, 34(10), 1283–1291. <https://doi.org/10.1016/j.advwatres.2011.06.006>
- Chegini, T., de Almeida Coelho, G., Ratcliff, J., Ferreira, C. M., Mandli, K., Burke, P., & Li, H.-Y. (2022). A novel framework for parametric analysis of coastal transition zone modeling. *JAWRA Journal of the American Water Resources Association*, 58(1), 86–103. <https://doi.org/10.1111/1752-1688.12983>
- Chen, W.-B., Liu, W.-C., & Wu, C.-Y. (2013). Coupling of a one-dimensional river routing model and a three-dimensional ocean model to predict overbank flows in a complex river-ocean system. *Applied Mathematical Modelling*, 37(9), 6163–6176. <https://doi.org/10.1016/j.apm.2013.01.003>

- Craig, A. P., Vertenstein, M., & Jacob, R. (2012). A new flexible coupler for Earth system modeling developed for CCSM4 and CESM1. *The International Journal of High Performance Computing Applications*, 26(1), 31–42. <https://doi.org/10.1177/1094342011428141>
- Danielson, J., Poppenga, S., Tyler, D., Palaseanu-Lovejoy, M., & Gesch, D. (2018). Coastal National Elevation Database (No. 2018–3037). <https://doi.org/10.3133/f20183037>
- Deb, M., Benedict, J. J., Sun, N., Yang, Z., Hetland, R., Judi, D., & Wang, T. (2023). Estuarine hurricane wind can intensify surge-dominated extreme water level in shallow and converging coastal systems. *EGUsphere*, 2023, 1–28.
- Deb, M., Sun, N., Yang, Z., Wang, T., Judi, D., Xiao, Z., & Wigmosta, M. S. (2023). Interacting effects of watershed and coastal processes on the evolution of compound flooding during Hurricane Irene. *Earth's Future*, 11(3), e2022EF002947. <https://doi.org/10.1029/2022ef002947>
- Desmet, K., Kopp, R. E., Kulp, S. A., Nagy, D. K., Oppenheimer, M., Rossi-Hansberg, E., & Strauss, B. H. (2018). *Evaluating the economic cost of coastal flooding* (Tech. Rep.). National Bureau of Economic Research.
- DiLorenzo, J. L., Huang, P., Thatcher, M. L., & Najarian, T. O. (1993). Dredging impacts on Delaware Estuary tides. In *Estuarine and coastal modeling* (pp. 86–104).
- Dykstra, S., & Dzwonkowski, B. (2020). The propagation of fluvial flood waves through a backwater-estuarine environment. *Water Resources Research*, 56(2), e2019WR025743. <https://doi.org/10.1029/2019wr025743>
- Egbert, G. D., & Erofeeva, S. Y. (2002). Efficient inverse modeling of barotropic ocean tides. *Journal of Atmospheric and Oceanic Technology*, 19(2), 183–204. [https://doi.org/10.1175/1520-0426\(2002\)019<0183:eimobo>2.0.co;2](https://doi.org/10.1175/1520-0426(2002)019<0183:eimobo>2.0.co;2)
- Eilander, D., Couasnon, A., Ikeuchi, H., Muis, S., Yamazaki, D., Winsemius, H. C., & Ward, P. J. (2020). The effect of surge on riverine flood hazard and impact in deltas globally. *Environmental Research Letters*, 15(10), 104007. <https://doi.org/10.1088/1748-9326/ab8ca6>
- Engwirda, D. (2017). JIGSAW-GEO (1.0): Locally orthogonal staggered unstructured grid generation for general circulation modelling on the sphere. *Geoscientific Model Development*, 10(6), 2117–2140. <https://doi.org/10.5194/gmd-10-2117-2017>
- Feng, D. (2024a). E3SM simulations of Hurricane Irene (Delaware River basin subset) [Dataset]. Zenodo. <https://doi.org/10.5281/zenodo.10616879>
- Feng, D. (2024b). E3SMv2 branch used for river-ocean two-way coupled ensemble simulations on variable-resolution meshes [Code]. Zenodo. <https://doi.org/10.5281/zenodo.10927690>
- Feng, D., Passalacqua, P., & Hodges, B. R. (2019). Innovative approaches for geometric uncertainty quantification in an operational oil spill modeling system. *Journal of Marine Science and Engineering*, 7(8), 259. <https://doi.org/10.3390/jmse7080259>
- Feng, D., Tan, Z., Engwirda, D., Liao, C., Xu, D., Bisht, G., et al. (2022). Investigating coastal backwater effects and flooding in the coastal zone using a global river transport model on an unstructured mesh. *Hydrology and Earth System Sciences*, 26(21), 5473–5491. <https://doi.org/10.5194/hess-26-5473-2022>
- Feng, D., Tan, Z., Xu, D., & Leung, L. R. (2023). Understanding the compound flood risk along the coast of the contiguous United States. *Hydrology and Earth System Sciences*, 27(21), 3911–3934. <https://doi.org/10.5194/hess-27-3911-2023>
- Golaz, J.-C., Caldwell, P. M., Van Roekel, L. P., Petersen, M. R., Tang, Q., Wolfe, J. D., et al. (2019). The DOE E3SM coupled model version 1: Overview and evaluation at standard resolution. *Journal of Advances in Modeling Earth Systems*, 11(7), 2089–2129. <https://doi.org/10.1029/2018ms001603>
- Golaz, J.-C., Van Roekel, L. P., Zheng, X., Roberts, A. F., Wolfe, J. D., Lin, W., et al. (2022). The DOE E3SM model version 2: Overview of the physical model and initial model evaluation. *Journal of Advances in Modeling Earth Systems*, 14(12). <https://doi.org/10.1029/2022ms003156>
- Gori, A., Lin, N., & Smith, J. (2020). Assessing compound flooding from landfalling tropical cyclones on the North Carolina coast. *Water Resources Research*, 56(4), e2019WR026788. <https://doi.org/10.1029/2019wr026788>
- Gori, A., Lin, N., Xi, D., & Emanuel, K. (2022). Tropical cyclone climatology change greatly exacerbates US extreme rainfall–surge hazard. *Nature Climate Change*, 12(2), 171–178. <https://doi.org/10.1038/s41558-021-01272-7>
- Gupta, H. V., Kling, H., Yilmaz, K. K., & Martinez, G. F. (2009). Decomposition of the mean squared error and NSE performance criteria: Implications for improving hydrological modelling. *Journal of Hydrology*, 377(1–2), 80–91. <https://doi.org/10.1016/j.jhydrol.2009.08.003>
- He, F., & Possehl, D. J. (2015). Impact of parameterized physical processes on simulated tropical cyclone characteristics in the community atmosphere model. *Journal of Climate*, 28(24), 9857–9872. <https://doi.org/10.1175/jcli-d-15-0255.1>
- Hermans, T. H., Malagón-Santos, V., Katsman, C. A., Jane, R. A., Rasmussen, D., Haasnoot, M., et al. (2023). The timing of decreasing coastal flood protection due to sea-level rise. *Nature Climate Change*, 13(4), 1–8. <https://doi.org/10.1038/s41558-023-01616-5>
- Hersbach, H., Bell, B., Berrisford, P., Hirahara, S., Horányi, A., Muñoz-Sabater, J., et al. (2020). The ERA5 global reanalysis. *Quarterly Journal of the Royal Meteorological Society*, 146(730), 1999–2049. <https://doi.org/10.1002/qj.3803>
- Huang, B., Liu, C., Banzon, V., Freeman, E., Graham, G., Hankins, B., et al. (2021). Improvements of the daily optimum interpolation sea surface temperature (DOISST) version 2.1. *Journal of Climate*, 34(8), 2923–2939. <https://doi.org/10.1175/jcli-d-20-0166.1>
- Ikeuchi, H., Hirabayashi, Y., Yamazaki, D., Muis, S., Ward, P. J., Winsemius, H. C., et al. (2017). Compound simulation of fluvial floods and storm surges in a global coupled river-coast flood model: Model development and its application to 2007 Cyclone Sidr in Bangladesh. *Journal of Advances in Modeling Earth Systems*, 9(4), 1847–1862. <https://doi.org/10.1002/2017ms000943>
- Intergovernmental Oceanographic Commission (IOC) of UNESCO and International Hydrographic Organization (IHO). (2020). General bathymetric chart of the oceans (GEBCO) digital Atlas. Retrieved from [https://www.gebco.net/data\\_and\\_products/gridded\\_bathymetry\\_data/](https://www.gebco.net/data_and_products/gridded_bathymetry_data/)
- Jongman, B., Ward, P. J., & Aerts, J. C. (2012). Global exposure to river and coastal flooding: Long term trends and changes. *Global Environmental Change*, 22(4), 823–835. <https://doi.org/10.1016/j.gloenvcha.2012.07.004>
- Karamouz, M., Razmi, A., Nazif, S., & Zahmatkesh, Z. (2017). Integration of inland and coastal storms for flood hazard assessment using a distributed hydrologic model. *Environmental Earth Sciences*, 76(11), 1–17. <https://doi.org/10.1007/s12665-017-6722-6>
- Kerns, B. W., & Chen, S. S. (2023). Compound effects of rain, storm surge, and river discharge on coastal flooding during Hurricane Irene and Tropical Storm Lee (2011) in the mid-Atlantic region: Coupled atmosphere-wave-ocean model simulation and observations. *Natural Hazards*, 116(1), 693–726. <https://doi.org/10.1007/s11069-022-05694-0>
- Kim, H. (2017). Global soil wetness project phase 3 atmospheric boundary conditions (experiment 1). (No Title).
- Knutson, T. R., Chung, M. V., Vecchi, G., Sun, J., Hsieh, T.-L., & Smith, A. J. (2021). Climate change is probably increasing the intensity of tropical cyclones. Critical issues in climate change science. *Science Brief Review*, 4570334. <https://doi.org/10.5281/zenodo>
- Kobayashi, S., Ota, Y., Harada, Y., Ebina, A., Moriya, M., Onoda, H., et al. (2015). The JRA-55 reanalysis: General specifications and basic characteristics. *Journal of the Meteorological Society of Japan Series II*, 93(1), 5–48. <https://doi.org/10.2151/jmsj.2015-001>
- Kulp, S. A., & Strauss, B. H. (2019). New elevation data triple estimates of global vulnerability to sea-level rise and coastal flooding. *Nature Communications*, 10(1), 1–12. <https://doi.org/10.1038/s41467-019-12808-z>
- Larson, J., Jacob, R., & Ong, E. (2005). The model coupling toolkit: A new Fortran90 toolkit for building multiphysics parallel coupled models. *The International Journal of High Performance Computing Applications*, 19(3), 277–292. <https://doi.org/10.1177/1094342005056115>

- Li, H.-Y., Ruby Leung, L., Tesfa, T., Voisin, N., Hejazi, M., Liu, L., et al. (2015). Modeling stream temperature in the Anthropocene: An earth system modeling approach. *Journal of Advances in Modeling Earth Systems*, 7(4), 1661–1679. <https://doi.org/10.1002/2015ms000471>
- Li, H.-Y., Tan, Z., Ma, H., Zhu, Z., Abeshu, G. W., Zhu, S., et al. (2022). A new large-scale suspended sediment model and its application over the United States. *Hydrology and Earth System Sciences*, 26(3), 665–688. <https://doi.org/10.5194/hess-26-665-2022>
- Liao, C., Zhou, T., Xu, D., Barnes, R., Bisht, G., Li, H.-Y., et al. (2022). Advances in hexagon mesh-based flow direction modeling. *Advances in Water Resources*, 160, 104099. <https://doi.org/10.1016/j.advwatres.2021.104099>
- Liao, C., Zhou, T., Xu, D., Cooper, M. G., Engwirda, D., Li, H.-Y., & Leung, L. R. (2023). Topological relationship-based flow direction modeling: Mesh-independent river networks representation. *Journal of Advances in Modeling Earth Systems*, 15(2), e2022MS003089. <https://doi.org/10.1029/2022ms003089>
- Liao, C., Zhou, T., Xu, D., Tan, Z., Bisht, G., Cooper, M. G., et al. (2023). Topological relationship-based flow direction modeling: Stream burning and depression filling. *Journal of Advances in Modeling Earth Systems*, 15(11), e2022MS003487. <https://doi.org/10.1029/2022ms003487>
- Lilly, J. R., Capodaglio, G., Petersen, M. R., Brus, S. R., Engwirda, D., & Higdon, R. L. (2023). Storm surge modeling as an application of local time-stepping in MPAS-ocean. *Journal of Advances in Modeling Earth Systems*, 15(1), e2022MS003327. <https://doi.org/10.1029/2022ms003327>
- Lin, N., & Chavas, D. (2012). On hurricane parametric wind and applications in storm surge modeling. *Journal of Geophysical Research*, 117(D9). <https://doi.org/10.1029/2011jd017126>
- Logemann, K., Linardakis, L., Korn, P., & Schrum, C. (2021). Global tide simulations with ICON-O: Testing the model performance on highly irregular meshes. *Ocean Dynamics*, 71(1), 43–57. <https://doi.org/10.1007/s10236-020-01428-7>
- Luo, X., Li, H.-Y., Leung, L. R., Tesfa, T. K., Getirana, A., Papa, F., & Hess, L. L. (2017). Modeling surface water dynamics in the Amazon basin using MOSART-inundation v1.0: Impacts of geomorphological parameters and river flow representation. *Geoscientific Model Development*, 10(3), 1233–1259. <https://doi.org/10.5194/gmd-10-1233-2017>
- Mandli, K. T., & Dawson, C. N. (2014). Adaptive mesh refinement for storm surge. *Ocean Modelling*, 75, 36–50. <https://doi.org/10.1016/j.ocemod.2014.01.002>
- Mathis, M., Logemann, K., Maerz, J., Lacroix, F., Hagemann, S., Chegini, F., et al. (2022). Seamless integration of the coastal ocean in global marine carbon cycle modeling. *Journal of Advances in Modeling Earth Systems*, 14(8), e2021MS002789. <https://doi.org/10.1029/2021ms002789>
- Morton, R. A., & Barras, J. A. (2011). Hurricane impacts on coastal wetlands: A half-century record of storm-generated features from southern Louisiana. *Journal of Coastal Research*, 27(6A), 27–43. <https://doi.org/10.2112/jcoastres-d-10-00185.1>
- Muis, S., Apecechea, M. I., Dullaart, J., de Lima Rego, J., Madsen, K. S., Su, J., et al. (2020). A high-resolution global dataset of extreme sea levels, tides, and storm surges, including future projections. *Frontiers in Marine Science*, 7, 263. <https://doi.org/10.3389/fmars.2020.00263>
- Najjar, R. G., Herrmann, M., Alexander, R., Boyer, E. W., Burdige, D., Butman, D., et al. (2018). Carbon budget of tidal wetlands, estuaries, and shelf waters of Eastern North America. *Global Biogeochemical Cycles*, 32(3), 389–416. <https://doi.org/10.1002/2017gb005790>
- Nasr, A. A., Wahl, T., Rashid, M. M., Camus, P., & Haigh, I. D. (2021). Assessing the dependence structure between oceanographic, fluvial, and pluvial flooding drivers along the United States coastline. *Hydrology and Earth System Sciences*, 25(12), 6203–6222. <https://doi.org/10.5194/hess-25-6203-2021>
- National Centers for Environmental Information. (2023). Coastal relief models (CRMs). <https://doi.org/10.25921/5ZN5-KN44>
- Neumann, B., Vafeidis, A. T., Zimmermann, J., & Nicholls, R. J. (2015). Future coastal population growth and exposure to sea-level rise and coastal flooding—a global assessment. *PLoS One*, 10(3), e0118571. <https://doi.org/10.1371/journal.pone.0118571>
- O'Neill, B. C., Tebaldi, C., Van Vuuren, D. P., Eyring, V., Friedlingstein, P., Hurtt, G., et al. (2016). The scenario model intercomparison project (ScenarioMIP) for CMIP6. *Geoscientific Model Development*, 9(9), 3461–3482. <https://doi.org/10.5194/gmd-9-3461-2016>
- Pal, N., Barton, K. N., Petersen, M. R., Brus, S. R., Engwirda, D., Arbic, B. K., et al. (2023). Barotropic tides in MPAS-ocean (E3SM V2): Impact of ice shelf cavities. *Geoscientific Model Development*, 16(4), 1297–1314. <https://doi.org/10.5194/gmd-16-1297-2023>
- Qiu, H., Bisht, G., Li, L., Hao, D., & Xu, D. (2023). Development of inter-grid cell lateral unsaturated and saturated flow model in the E3SM land model (v2.0). *EGUphere*, 2023, 1–31.
- Rappaport, E. N. (2000). Loss of life in the United States associated with recent Atlantic tropical cyclones. *Bulletin of the American Meteorological Society*, 81(9), 2065–2074. [https://doi.org/10.1175/1520-0477\(2000\)081<2065:lolit>2.3.co;2](https://doi.org/10.1175/1520-0477(2000)081<2065:lolit>2.3.co;2)
- Santiago-Collazo, F. L., Bilskie, M. V., & Hagen, S. C. (2019). A comprehensive review of compound inundation models in low-gradient coastal watersheds. *Environmental Modelling and Software*, 119, 166–181. <https://doi.org/10.1016/j.envsoft.2019.06.002>
- Sharp, J. H. (1984). *Excerpts from the Delaware estuary: Research as background for estuarine management and development: A report to the Delaware River and bay authority*. University of Delaware, Sea Grant College Program.
- Sheng, P. Y., Paramygin, V. A., Yang, K., & Rivera-Nieves, A. A. (2022). A sensitivity study of rising compound coastal inundation over large flood plains in a changing climate. *Scientific Reports*, 12(1), 3403. <https://doi.org/10.1038/s41598-022-07010-z>
- Strauss, B. H., Orton, P. M., Bittermann, K., Buchanan, M. K., Gilford, D. M., Kopp, R. E., et al. (2021). Economic damages from Hurricane Sandy attributable to sea level rise caused by anthropogenic climate change. *Nature Communications*, 12(1), 2720. <https://doi.org/10.1038/s41467-021-22838-1>
- Sun, N., Wigmosta, M. S., Judi, D., Yang, Z., Xiao, Z., & Wang, T. (2021). Climatological analysis of tropical cyclone impacts on hydrological extremes in the Mid-Atlantic region of the United States. *Environmental Research Letters*, 16(12), 124009. <https://doi.org/10.1088/1748-9326/ac2d6a>
- Talke, S. A., & Jay, D. A. (2020). Changing tides: The role of natural and anthropogenic factors. *Annual Review of Marine Science*, 12(1), 121–151. <https://doi.org/10.1146/annurev-marine-010419-010727>
- Tan, Z., Leung, L. R., Li, H.-Y., Tesfa, T., Zhu, Q., Yang, X., et al. (2021). Increased extreme rains intensify erosional nitrogen and phosphorus fluxes to the northern Gulf of Mexico in recent decades. *Environmental Research Letters*, 16(5), 054080. <https://doi.org/10.1088/1748-9326/abf006>
- Tellman, B., Sullivan, J., Kuhn, C., Kettner, A., Doyle, C., Brakenridge, G., et al. (2021). Satellite imaging reveals increased proportion of population exposed to floods. *Nature*, 596(7870), 80–86. <https://doi.org/10.1038/s41586-021-03695-w>
- Towner, J., Cloke, H. L., Zsoter, E., Flamig, Z., Hoch, J. M., Bazo, J., et al. (2019). Assessing the performance of global hydrological models for capturing peak river flows in the Amazon basin. *Hydrology and Earth System Sciences*, 23(7), 3057–3080. <https://doi.org/10.5194/hess-23-3057-2019>
- Ullrich, P. A., Devendran, D., & Johansen, H. (2016). Arbitrary-order conservative and consistent remapping and a theory of linear maps: Part II. *Monthly Weather Review*, 144(4), 1529–1549. <https://doi.org/10.1175/mwr-d-15-0301.1>

- Ullrich, P. A., & Taylor, M. A. (2015). Arbitrary-order conservative and consistent remapping and a theory of linear maps: Part I. *Monthly Weather Review*, 143(6), 2419–2440. <https://doi.org/10.1175/mwr-d-14-00343.1>
- Ward, N. D., Bianchi, T. S., Medeiros, P. M., Seidel, M., Richey, J. E., Keil, R. G., & Sawakuchi, H. O. (2017). Where carbon goes when water flows: Carbon cycling across the aquatic continuum. *Frontiers in Marine Science*, 4, 7. <https://doi.org/10.3389/fmars.2017.00007>
- Ward, N. D., Megonigal, J. P., Bond-Lamberty, B., Bailey, V. L., Butman, D., Canuel, E. A., et al. (2020). Representing the function and sensitivity of coastal interfaces in Earth system models. *Nature Communications*, 11(1), 2458. <https://doi.org/10.1038/s41467-020-16236-2>
- Ward, P. J., Couasnon, A., Eilander, D., Haigh, I. D., Hendry, A., Muis, S., et al. (2018). Dependence between high sea-level and high river discharge increases flood hazard in global deltas and estuaries. *Environmental Research Letters*, 13(8), 084012. <https://doi.org/10.1088/1748-9326/aad400>
- Whitney, M. M., & Garvine, R. W. (2006). Simulating the Delaware Bay buoyant outflow: Comparison with observations. *Journal of Physical Oceanography*, 36(1), 3–21. <https://doi.org/10.1175/jpo2805.1>
- Wong, K.-C., & Sommerfield, C. K. (2009). The variability of currents and sea level in the upper Delaware estuary. *Journal of Marine Research*, 67(4), 479–501. <https://doi.org/10.1357/002224009790741111>
- Xiao, Z., Yang, Z., Wang, T., Sun, N., Wigmosta, M., & Judi, D. (2021). Characterizing the non-linear interactions between tide, storm surge, and river flow in the Delaware bay estuary, United States. *Frontiers in Marine Science*, 8, 715557. <https://doi.org/10.3389/fmars.2021.715557>
- Xu, D., Bisht, G., Sargsyan, K., Liao, C., & Leung, L. R. (2022). Using a surrogate-assisted Bayesian framework to calibrate the runoff-generation scheme in the energy exascale Earth system model (E3SM) v1. *Geoscientific Model Development*, 15(12), 5021–5043. <https://doi.org/10.5194/gmd-15-5021-2022>
- Xu, D., Bisht, G., Zhou, T., Leung, L. R., & Pan, M. (2022). Development of land-river two-way hydrologic coupling for floodplain inundation in the energy exascale Earth system model. *Journal of Advances in Modeling Earth Systems*, 14(8), e2021MS002772. <https://doi.org/10.1029/2021ms002772>
- Xu, K., Wang, C., & Bin, L. (2023). Compound flood models in coastal areas: A review of methods and uncertainty analysis. *Natural Hazards*, 116(1), 469–496. <https://doi.org/10.1007/s11069-022-05683-3>
- Yamazaki, D., Lee, H., Alsdorf, D. E., Dutra, E., Kim, H., Kanae, S., & Oki, T. (2012). Analysis of the water level dynamics simulated by a global river model: A case study in the Amazon River. *Water Resources Research*, 48(9). <https://doi.org/10.1029/2012wr011869>
- Ye, F., Zhang, Y. J., Yu, H., Sun, W., Moghimi, S., Myers, E., et al. (2020). Simulating storm surge and compound flooding events with a creek-to-ocean model: Importance of baroclinic effects. *Ocean Modelling*, 145, 101526. <https://doi.org/10.1016/j.ocemod.2019.101526>
- Zarzycki, C. M., & Jablonowski, C. (2015). Experimental tropical cyclone forecasts using a variable-resolution global model. *Monthly Weather Review*, 143(10), 4012–4037. <https://doi.org/10.1175/mwr-d-15-0159.1>
- Zarzycki, C. M., Jablonowski, C., & Taylor, M. A. (2014). Using variable-resolution meshes to model tropical cyclones in the Community Atmosphere Model. *Monthly Weather Review*, 142(3), 1221–1239. <https://doi.org/10.1175/mwr-d-13-00179.1>
- Zender, C. S. (2008). Analysis of self-describing gridded geoscience data with netCDF Operators (NCO). *Environmental Modelling and Software*, 23(10–11), 1338–1342. <https://doi.org/10.1016/j.envsoft.2008.03.004>
- Zhang, Y. J., Fernandez-Montblanc, T., Pringle, W., Yu, H.-C., Cui, L., & Moghimi, S. (2023). Global seamless tidal simulation using a 3D unstructured-grid model (SCHISM v5. 10.0). *Geoscientific Model Development*, 16(9), 2565–2581. <https://doi.org/10.5194/gmd-16-2565-2023>
- Zhang, Y. J., Ye, F., Yu, H., Sun, W., Moghimi, S., Myers, E., et al. (2020). Simulating compound flooding events in a hurricane. *Ocean Dynamics*, 70(5), 621–640. <https://doi.org/10.1007/s10236-020-01351-x>
- Zscheischler, J., Martius, O., Westra, S., Bevacqua, E., Raymond, C., Horton, R. M., et al. (2020). A typology of compound weather and climate events. *Nature Reviews Earth & Environment*, 1(7), 333–347. <https://doi.org/10.1038/s43017-020-0060-z>